FI SEVIER

Contents lists available at ScienceDirect

Commun Nonlinear Sci Numer Simulat

journal homepage: www.elsevier.com/locate/cnsns



Research paper

Deformation and coalescence of ferrodroplets in Rosensweig model using the phase field and modified level set approaches under uniform magnetic fields



Feng Bai^{a,c}, Daozhi Han^b, Xiaoming He^{b,*}, Xiaofeng Yang^c

- ^a Department of Mechanical Engineering, University of South Carolina, 300 Main Street, Columbia, S.C. 29208, USA
- b Department of Mathematics and Statistics, Missouri University of Science and Technology, 400 W. 12th Street, Rolla, Mo 65409, USA
- ^c Department of Mathematics, University of South Carolina, 1523 Greene Street, Columbia, S.C. 29208, USA

ARTICLE INFO

Article history: Received 3 August 2018 Revised 23 January 2020 Accepted 28 January 2020 Available online 5 February 2020

Keywords:
Ferrodroplet
Deformation and coalescence
Rosensweig model
Phase field approach
Modified level set approach
Finite element method

ABSTRACT

By using both a phase field approach and a modified level set approach, two multiphase numerical models are proposed and compared in this paper to investigate the ferrodroplet deformation and merging process in a non-magnetic viscous medium under the influence of uniform magnetic fields. The finite element method is utilized for the spatial discretization of both numerical models. The numerical results show excellent agreement with the analytical solutions in the simple axisymmetric setting. The effects of different magnetic bond numbers and magnetic susceptibility on the deformation of ferrodroplets are systematically investigated. The coalescence process, in which two small ferrodroplets merge into a single larger droplet under uniform magnetic fields, is also studied by using both the phase field approach and the modified level set approach. Moreover the attraction phenomenon between two ferrodroplets, which was previously discovered in numerical experiments, is observed in our numerical tests. By comparing with analytical solutions, our study demonstrates that the diffuse interface (phase field) approach performs better than the modified level set approach when there is large topological deformation of the ferrodroplet. Several other important aspects, including the evolution of the flow field, the magnetic energy distribution, the spurious flows near the interfaces, and conservation of mass in both approaches, are studied as well.

© 2020 Elsevier B.V. All rights reserved.

1. Introduction

Droplet deformations in two immiscible fluids system with physical effects such as hydraulic, electric or magnetic, etc. on the interface are widely investigated by using numerical and experimental approaches. The principal mechanism for the deformation is capillary forces acting on the interface between the two immiscible fluids [1,2]. Bubbles/droplets can experience shape deformations under the hydraulic forces on the interface in a shear flow and sometimes the breakup of bubbles/droplets could be observed in situations of large shear forces [3,4]. Recently the electrohydrodynamic (EHD) deformations of droplet/bubble with external electric fields have been studied extensively, with results including the discovery of the slender shape [5], the deformations of droplets in strong electric fields [6], the oblate shape of nonlinear electrohy-

^{*} Corresponding author. E-mail address: hex@mst.edu (X. He).

drodynamic deformations [7], the inertia effect on the deformed shape under electric fields [8], the stable shape of droplets in nonlinear electrical polarization [9], and the droplet deformations in AC electric fields [10]. In addition to these electrohydrodynamic deformations, the breakup and burst phenomena in electric fields are also observed both experimentally [11,12] and numerically [13,14].

Ferrohydrodynamics(FHD) is a fundamental yet challenging research topic with a wide range of applications in engineering and pharmaceutical fields where the ferrofluids could be directly controlled by magnetic fields. One of special interests is the ferrodroplet deformations and instability under uniform magnetic fields which was previously examined by a number of authors [15–17]. Since then, the single-phase ferrofluid problem has been studied by using either the classic Rosensweig type model [18–20] or the simplified Shliomis model [21]. The so-called Rosensweig interfacial instability under external magnetic fields is reported in both experiments [22,23] and numerical simulations [24,25]. Interfacial instability under magnetic fields is also studied in the context of thin film ferrofluid interacting with non-magnetic viscous fluid [26–28]. Numerical simulations have been playing an increasingly important role in the study of ferrodroplet deformations and instabilities, and new phenomena, such as ferrodrop transient movements, elongated shape of ferrodroplet along magnetic fields, dynamic deformations combining magnetic effects, inertia and viscosity, are reported in concurrent literature [29–31].

There are several well-known approaches for numerical simulations of multi-phase flows, cf. [32] for a comprehensive review, such as the front-tracking method [33,34], volume of fluid (VOF) method [29,30,35–40], level set approach [41–47], phase field approach [48–60], etc. The level-set method uses a level-set function to represent the shape of the dynamic interface and has been used to study the effects of magnetic fields on the interface between two-phase incompressible flows [61–63] and dynamic motions of dielectric bubble under uniform magnetic fields [64]. The Phase-field /diffuse-interface approach treats the interface as a transition layer of finite thickness where the two fluids "mix" to a certain degree. The overall hydrodynamics of the multiphase fluid system in this phase-field framework is the result of competitions between the kinetic energy and the elastic mixing energy. In recent years, this method has been used to study different two-phase flow problems and liquid crystal problems, see [65–81] and references therein.

While many works have been devoted to different methods for single-phase ferrofluids or single-phase magnetohydrodynamics (MHD) [18–21,82–100], more research needs to be done for two-phase ferrofluids or two-phase MHD flows, see [29–31,61,62,101,102] and references therein for some initial development in this direction. In this contribution, we propose and compare two numerical two-phase flow models based on the phase field approach and regularized level-set approach for simulations of ferrodroplet deformation under the influence of uniform magnetic fields. Both methods can well capture the deformation of the ferrodroplet. The diffuse interface model has the advantage of being able to seamlessly capture topological transitions of the interface such as droplet merging without suffering loss of accuracy, in contrast to the ad-hoc nature (artificial diffusion) of the level-set approach in dealing with droplet merging. Compared with the phase field model proposed recently in [101] where matched densities are assumed for the two phases, our models deal with two-phase ferrofluids of different densities. Ample numerical experiments are performed to illustrate the effects of problem parameters on the ferrodroplet deformation and to support the comparison between the two numerical models.

The rest of this paper is organized as follows. In Section 2 a Rosensweig model by the phase field approach is introduced. In Section 3 another Rosensweig model using the modified level set approach is presented. In Section 4, we discuss the model configuration, the physical parameters, and the setup for numerical experiments. In Section 5, several numerical experiments are performed to illustrate the features of the proposed models, including the deformation and coalescence phenomena.

2. A Rosensweig model using phase field approach

In [101], a new phase field model was proposed for the two-phase ferrohydradynamics. Based on the idea in [101], we propose a new model for two-phase flows of different densities. Assuming that the two-phase fluids are immiscible and incompressible, the phase field model introduces a phase-field function $\phi(\mathbf{x}, t)$ to identify the magnetic phase and the nonmagnetic phase:

$$\phi(\mathbf{x},t) = \begin{cases} 1, & \text{non-magnetic medium,} \\ -1, & \text{ferrofluid droplet.} \end{cases}$$
 (1)

There is a thin transition region of width ε between the two phases. In this transition region the phase-field function varies continuously and smoothly from $\phi = -1$ to $\phi = 1$ with the zero level set $\Gamma_t = \{x : \phi(x, t) = 0\}$ in the middle of the transition region.

The mixing energy in the transition layer is defined as [50,103]

$$E_{mix}(\phi) = \int_{\Omega} K\left(\frac{1}{2}|\nabla\phi|^2 + F(\phi)\right) d\mathbf{x},\tag{2}$$

where $F(\phi) = \frac{1}{4\varepsilon^2}(\phi^2 - 1)^2$ is the homogeneous free energy density function that has a profile of double-well potential. The first term contributes to the hydrophilic type(tendency of mixing) of interactions between materials, while the second term represents the hydrophobic type (tendency of separation) of interactions between two phases. The equilibrium between the two types of interaction leads to the balance of the energy at the diffuse interface with a thickness parameter ε . K is the

mixing energy density which is related to the interfacial thickness ε and the surface tension coefficient σ as follows [53]

$$\sigma = \frac{2\sqrt{2}}{3} \frac{K}{\varepsilon}.$$
 (3)

This relationship between the energy density and surface tension needs to hold in the sharp interface limit. As the interfacial thickness shrinks to zero, the energy density will decrease to zero in order to keep the surface tension as a constant physical value. The chemical potential $G = \frac{\partial E_{mix}}{\partial \phi}$ represents the change rate of the mixing energy and the expression is:

$$G = -K\nabla^2 \phi + f(\phi). \tag{4}$$

where $f(\phi) = F'(\phi) = u\phi^3 - r\phi$. r, u are the computational parameters obtained from molecular dynamics (MD) simulations with a relationship of $r = u = \frac{K}{c^2}$. In view of the relation (3) one can express the chemical potential as

$$G = \frac{3\varepsilon\sigma}{2\sqrt{2}} \left(-\nabla^2\phi + \frac{\phi(\phi^2 - 1)}{\varepsilon^2} \right). \tag{5}$$

Then the phase-field function is governed by the following advective Cahn-Hilliard equation [104]:

$$\begin{cases}
\frac{\partial \phi}{\partial t} + \nabla \cdot (\mathbf{u}\phi) = M\nabla^2 G, \\
G = \frac{3\varepsilon\sigma}{2\sqrt{2}} \left(-\nabla^2 \phi + \frac{\phi(\phi^2 - 1)}{\varepsilon^2} \right),
\end{cases} (6)$$

where M is a phenomenological mobility parameter which determines the relaxation time of interface in the Cahn–Hilliard equation [53]. Its value is proportional to square of the interfacial thickness $M = \chi_{mo} \varepsilon^2$, where χ_{mo} is the tuning mobility parameter [105].

In the diffuse interface method, the physical properties for the two incompressible complex fluids vary smoothly with the phase-field function ϕ :

$$\begin{cases}
\rho(\phi) = \frac{1}{2} \left[(1 - \phi) \cdot \rho_f + (1 + \phi) \cdot \rho_n \right], \\
\eta(\phi) = \frac{1}{2} \left[(1 - \phi) \cdot \eta_f + (1 + \phi) \cdot \eta_n \right].
\end{cases}$$
(7)

where ρ_f is the density of ferrofluid, ρ_n is the density of non-magnetic fluid, η_f is the viscosity of ferrofluid, and η_n is the viscosity of non-magnetic fluid, respectively. Then the momentum equation for the fluid flow in the phase field model is, cf.[50,53,106]:

$$\begin{cases} \rho \left[\frac{\partial \mathbf{u}}{\partial t} + (\mathbf{u} \cdot \nabla) \mathbf{u} \right] + J \cdot \nabla \mathbf{u} = -\nabla p + \nabla \cdot \eta \left(\nabla \mathbf{u} + \nabla \mathbf{u}^T \right) + G \nabla \phi + \nabla \cdot \boldsymbol{\tau}_m + \mathbf{F}_{ext}, \\ \nabla \cdot \mathbf{u} = 0, \end{cases}$$
(8)

where $J = -\frac{\Delta \rho}{2}M\nabla G$ with $\Delta \rho = \rho_n - \rho_f$, \boldsymbol{u} is the velocity vector, p is the pressure and \boldsymbol{F}_{ext} is used to demonstrate the external body force such as buoyancy or gravity. In our study, both of the two-phase fluids are incompressible and the external force is neglected. The term $\nabla \cdot \eta \left(\nabla \boldsymbol{u} + \nabla \boldsymbol{u}^T \right)$ represents the effect of viscosity and the term $G\nabla \phi$ gives rise to capillarity (surface tension) of the two-phase complex fluids system [50].

Since the two-phase fluids are assumed to be incompressible, isothermal and the ferrofluid is linearly magnetizable, the magnetic stress tensor at the interface could be expressed as [30,62]:

$$\boldsymbol{\tau}_{m} = -\frac{\mu(\boldsymbol{\phi})}{2} H^{2} \mathbf{I} + \mu(\boldsymbol{\phi}) \mathbf{H} \mathbf{H}^{T}, \tag{9}$$

where H = |H| is the norm of magnetic strength and I denotes the identity matrix. Then the magnetic stress tensor at the diffuse interface could be transformed to the magnetic body force $\nabla \cdot \tau_m$ by using the divergence theorem and is added into the momentum equation. The magnetic permeability μ for the two phase fluids is also defined in terms of the phase-field function ϕ :

$$\mu(\phi) = \frac{1}{2} ((1 - \phi) \cdot \mu_f + (1 + \phi) \cdot \mu_n). \tag{10}$$

The permeability of ferrofluid is $\mu_f = \mu_0(1 + \chi_f)$ and the permeability of non-magnetic fluid is $\mu_n = \mu_0(1 + \chi_n)$, where χ_f and χ_n represent the magnetic susceptibility of ferrodroplet and non-magnetic viscous medium, respectively.

The magnetic field is governed by the following Maxwell equation following the collinear assumption in [18,19]:

$$\begin{cases} \nabla \cdot \mathbf{B} = 0 \\ \nabla \times \mathbf{H} = 0, \end{cases} \tag{11}$$

where $\boldsymbol{\mathit{B}}$ denotes the magnetic induction which could be written as:

$$\mathbf{B} = \begin{cases} \mu_f \mathbf{H}, & \text{in ferrofluid} \\ \mu_n \mathbf{H}, & \text{in non-ferrofluid.} \end{cases}$$
 (12)

We define ψ as the magnetic scalar potential function such that $\mathbf{H} = -\nabla \psi$. Then the Maxwell equation can be rewritten as:

$$-\nabla \cdot (\mu(\phi)\nabla\psi) = 0. \tag{13}$$

3. A Rosensweig model by a modified level set approach

In the classical level set approach, the level set function is chosen to be the singed distance function [107]. A smeared out Heaviside function (of the level set function) is often employed for robust computations of density and viscosity discontinuities over the interface. Following [46,47], we collapse these two steps and introduce a modified level set function Φ to describe the phase distribution in the two-phase incompressible fluid system. The function Φ , which is our modified level set function and similar to the phase field function, takes values:

$$\Phi = \begin{cases}
0, & \text{ferrodroplet,} \\
1, & \text{non-ferrofluid,}
\end{cases}$$
(14)

and a sharp interface can be defined as the 0.5 level set of Φ .

In previous literatures [46,47] the authors realize the advection of the level set function Φ at one time step by first solving an advection equation for Φ , as in the standard modified level set approach, followed by solving a relaxed conservation law to equilibrium so as to maintain the thickness and shape of the interface. In this way the property of conservation of area is achieved at the expense of increased computational cost. In our modified level set approach, we consider to solve the following equation in order to reduce the computational cost and improve the efficiency:

$$\frac{\partial \Phi}{\partial t} + \nabla \cdot (\mathbf{u}\Phi) + \nabla \cdot L(\Phi) = \epsilon \Delta \Phi \tag{15}$$

where $L(\Phi) = \Phi(1-\Phi) \mathbf{n}$ is an artificial compressive flux for preserving the shape and the thickness of the interface. Such an artificial compressive flux counterbalances the diffusive flux. In general one expects the introduction of mass error due to the $L(\Phi)$ contribution. In our simulations only pure phases are present on the boundary (interfaces away from the boundary). Hence the total mass is still conserved. In this equation ϵ is the interface parameter which is representing the interfacial thickness in the modified level set approach, $\mathbf{n} = \frac{\nabla \Phi}{|\nabla \Phi|}$ is the unit normal vector whose direction is perpendicular to the two-phase interface, and the contour line at $\Phi = 0.5$ corresponds to the centered line of the sharp interface. The variations of physical properties inside the interface of the complex fluids could be demonstrated by using the level set function as follows:

$$\begin{cases}
\rho(\Phi) = \rho_n + (\rho_f - \rho_n) \cdot \Phi, \\
\eta(\Phi) = \eta_n + (\eta_f - \eta_n) \cdot \Phi, \\
\mu(\Phi) = \mu_n + (\mu_f - \mu_n) \cdot \Phi.
\end{cases} \tag{16}$$

where ρ , η , μ are the density, the viscosity and the magnetic permeability of the two phase fluids. By neglecting the external body forces such as buoyancy ($F_b \approx 0$) and gravity forces ($F_g \approx 0$), the momentum equations of two-phase fluids for the level set model are:

$$\begin{cases} \rho \left[\frac{\partial \mathbf{u}}{\partial t} + (\mathbf{u} \cdot \nabla) \mathbf{u} \right] = \nabla \cdot \left[-p\mathbf{I} + \eta \left(\nabla \mathbf{u} + \nabla \mathbf{u}^T \right) \right] + \mathbf{F}_s + \mathbf{F}_m, \\ \nabla \cdot \mathbf{u} = 0 \end{cases}$$
(17)

In the momentum equation the surface tension effect and the magnetic effect are treated as body forces: the surface tension force \mathbf{F}_s and the magnetic force \mathbf{F}_m which are defined respectively as:

$$\begin{cases}
\mathbf{F}_{s} = \nabla \cdot \left[\sigma \left(\mathbf{I} - (\mathbf{n} \mathbf{n}^{T}) \right) \delta \right], \\
\mathbf{F}_{m} = \nabla \cdot \left[-\frac{\mu(\Phi)}{2} H^{2} \mathbf{I} + \mu(\Phi) \mathbf{H} \mathbf{H}^{T} \right],
\end{cases}$$
(18)

where $\delta = 6|\nabla\Phi||\Phi(1-\Phi)|$ is an approximation of the surface Dirac delta function [108]. Moreover, the magnetic equations can be expressed as the following [18,19]:

$$\begin{cases}
\boldsymbol{\tau}_{m} = -\frac{\mu(\Phi)}{2}H^{2}\mathbf{I} + \mu(\Phi)\mathbf{H}\mathbf{H}^{T}, \\
-\nabla \cdot (\mu(\Phi)\nabla\psi) = 0, \\
\mu(\Phi) = \mu_{n} + (\mu_{f} - \mu_{n}) \cdot \Phi,
\end{cases} \tag{19}$$

where $\nabla \cdot \tau_m$ is the transformed magnetic body force by the divergence theorem exerting on the two-phase fluids in the momentum equation. It should be noted that in the Maxwell equation the magnetic distribution is associated with the level set variable (Φ) .

4. Preparation for the numerical experiments

Based on the two models presented in the previous two sections, we will perform numerical experiments and discuss the results in the following sections. The next section is devoted to the set-up of the numerical experiments.

4.1. Model configuration

The 2D axisymmetric configuration of the ferrodroplet deformation system is shown in Fig. 1. The whole computational domain Ω is set to be a cylinder with the outer radius $R_L = 5$ mm and the height $H_L = 20$ mm. The initial ferrodroplet is

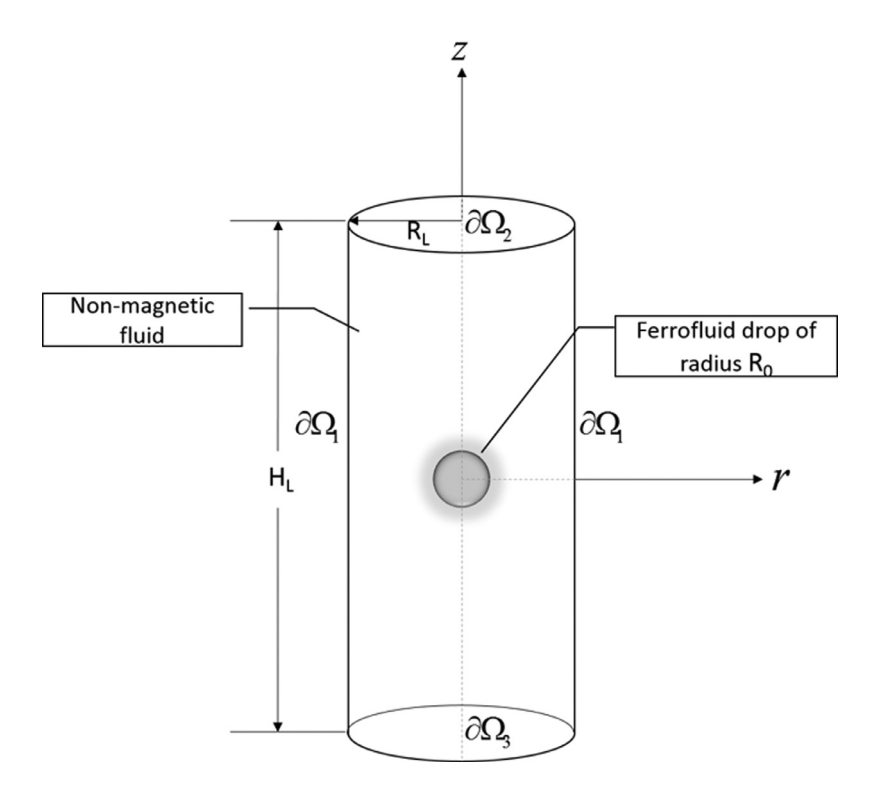


Fig. 1. The 3D schematic of ferrodroplet deformation configuration in external uniform magnetic fields.

located in the center of the cylindrical domain with its radius $R_0 = 1$ mm which is also treated as the characteristic radius of droplet. The rest part of the computational domain is filled with the non-magnetic viscous fluid. The external magnetic field is assumed to be uniformly distributed in the axisymmetric geometry with its direction from the bottom of the cylinder to the top.

The boundary conditions for the model system are defined as follows. For the magnetic scalar potential ψ , Neumann boundary condition is utilized on boundary $\partial\Omega_1$ and Dirichlet boundary conditions are chosen on boundaries $\partial\Omega_2$ and $\partial\Omega_3$:

$$\begin{cases} \partial_{\mathbf{n}} \psi |_{\partial \Omega_{1}} = 0, \\ \psi |_{\partial \Omega_{2}} = 0, \\ \psi |_{\partial \Omega_{3}} = \psi_{b0} * \beta(t). \end{cases}$$
 (20)

Here ψ_{b0} is a fixed value and $\beta(t)$ is a function which smoothly increases from 0 to 1 in 20 ms (0.02 s) and stays at 1 after that. For the velocity, the no-penetration and free-slip boundary condition is applied on the boundary $\partial\Omega_1$ and the no-slip no penetration boundary condition is applied on $\partial\Omega_2$ and $\partial\Omega_3$:

$$\begin{cases}
\partial_{\mathbf{n}} \mathbf{u}_{\tau}|_{\partial \Omega_{1}} = 0, \\
\mathbf{u} \cdot \mathbf{n}|_{\partial \Omega_{1}} = 0, \\
\mathbf{u}|_{\partial \Omega_{2}} = 0, \\
\mathbf{u}|_{\partial \Omega_{3}} = 0.
\end{cases}$$
(21)

The above boundary conditions are valid for both the phase field model and the level set model. For the phase field function ϕ and the chemical potential G in the phase field model, the homogeneous Neumann condition is applied:

$$\begin{cases} \partial_{n} \phi |_{\partial \Omega} = 0, \\ \partial_{n} G |_{\partial \Omega} = 0. \end{cases}$$
 (22)

For the level set function Φ in the level set model, the homogeneous Neumann condition is applied:

$$\partial_{\mathbf{n}}\Phi|_{\partial\Omega}=0$$
 (23)

The phase variable ϕ is determined by phase initialization and time dependent evolution in the Cahn–Hilliard equation (Eq. (6)). The phase initialization condition is expressed as follows:

$$\phi_0 = \begin{cases} -tanh\left(\frac{D_h}{\sqrt{2}\varepsilon}\right), & \text{for ferrofluid drop,} \\ tanh\left(\frac{D_h}{\sqrt{2}\varepsilon}\right), & \text{for non-magnetic medium,} \end{cases}$$
 (24)

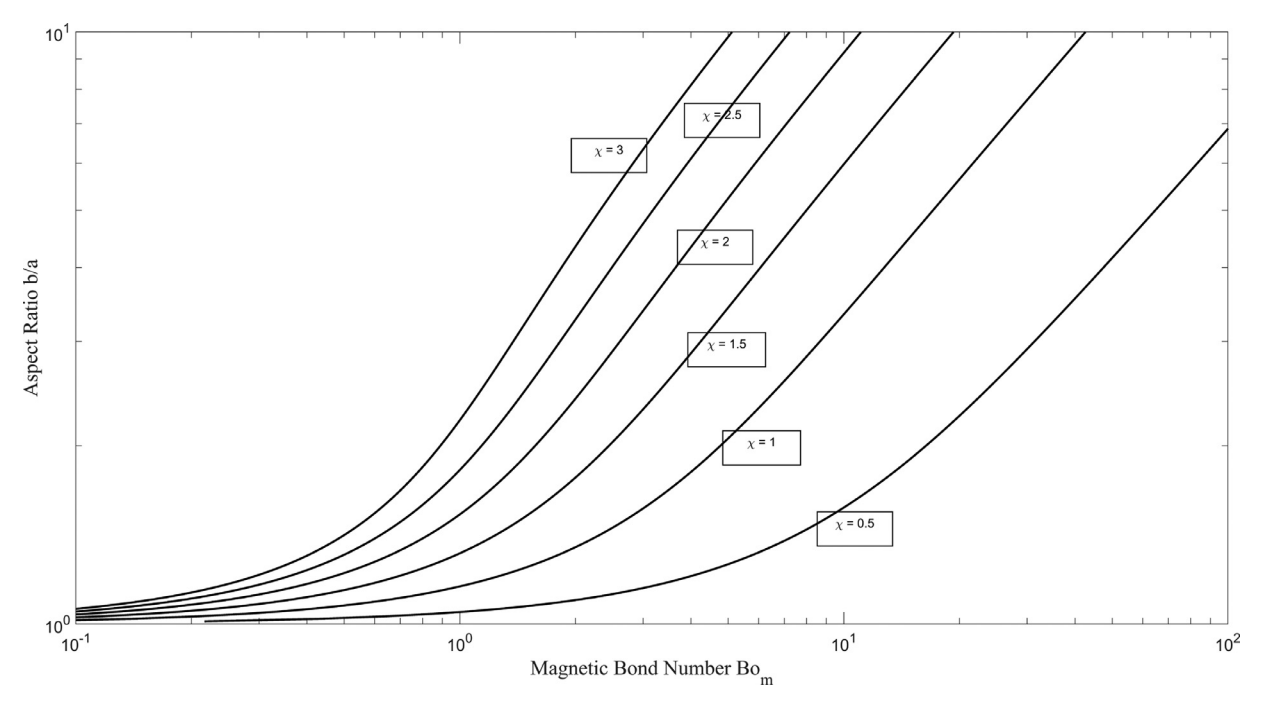


Fig. 2. In the analytical solutions the aspect ratio $\gamma = b/a$ at equilibrium state is a function of the magnetic bond number Bo_m with different values of magnetic susceptibility in ferrofluid $\chi_f = 0.5, 1, 1.5, 2, 2.5, 3$.

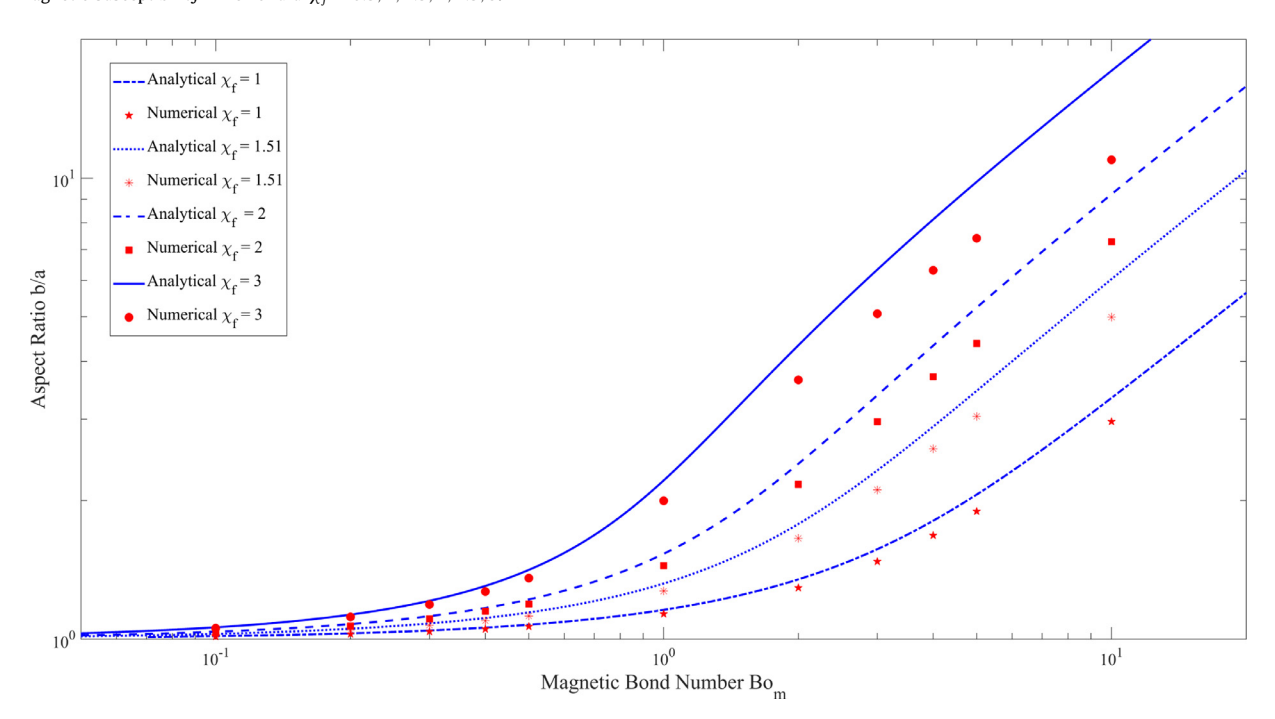


Fig. 3. The comparison of equilibrium drop aspect ratio between numerical results of the Rosensweig model with phase field approach and the analytical solution by using different values of magnetic susceptibility ($\chi_f = 1$, $\chi_f = 1.51$, $\chi_f = 2$ and $\chi_f = 3$) with the variation of magnetic bond number. Other physical properties are the same as the Silicone-EMG707 system.

where D_h is the distance between the location of phase variable and the initial interface ($\phi_0 = 0$).

The level set function is determined by function initialization and time dependent evolution in the level set equation. The level set function initialization condition is expressed as follows:

$$\Phi_0 = \begin{cases} \frac{1}{1 + e^{-D_h/\varepsilon}}, & \text{for ferrofluid drop,} \\ \frac{1}{1 + e^{D_h/\varepsilon}}, & \text{for non-magnetic medium,} \end{cases}$$
(25)

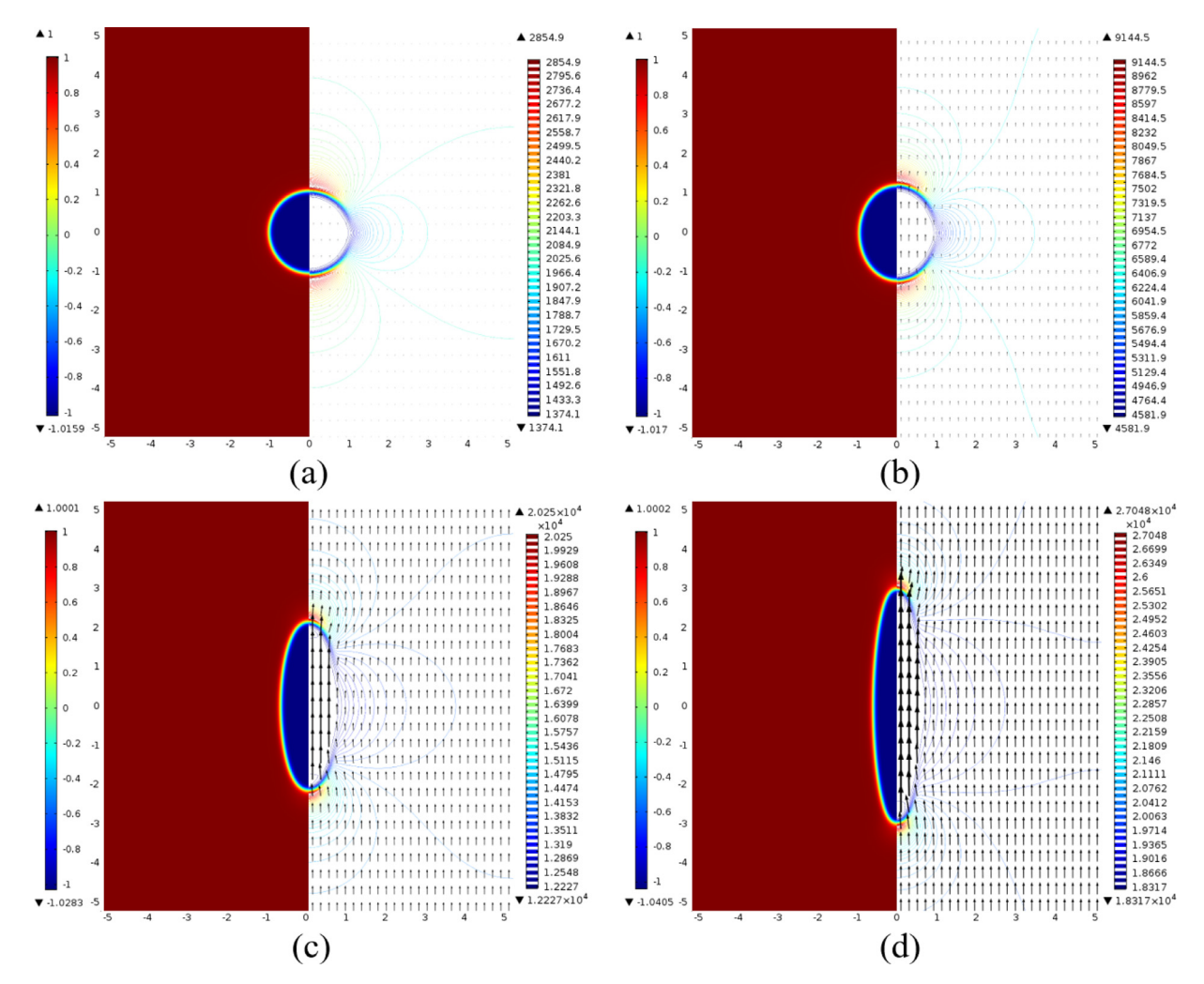


Fig. 4. The 2D cross-section shapes of ferrodroplet(left) and the magnetic field distributions(right) in the final quasi-equilibrium state T = 0.1 s with four different values of magnetic bond number: (a) $Bo_m = 0.1$, (b) $Bo_m = 1$, (c) $Bo_m = 5$ and (d) $Bo_m = 10$ in the real Silicon-EMG707 system ($\chi_f = 1.51$). The contour distributions shown are for the magnetic field strength \mathbf{H} and the arrows indicate the strength and the directions of magnetic induction \mathbf{B} .

where D_h is the distance between the location of level set function and the initial interface ($\Phi_0 = 0.5$).

In this paper we focus on the deformation of ferrodroplet under the influence of magnetic effect and surface tension effect between ferrofluid and non-magnetic medium by using the two Rosensweig models presented in the previous two sections. The important characteristic parameters in this model system will be discussed in the following subsection.

4.2. Characteristic parameters

In the phase field model the mixing energy E_{mix} in the Cahn-Hilliard equation is associated with the interfacial thickness ε . The Cahn number $Cn = \varepsilon/R_0$ denotes the dimensionless ratio between the thickness of the diffuse interface to the spherical droplet radius to represent the relative interfacial thickness. In the Rosensweig model the with phase field approach, the Cahn number is fixed as Cn = 0.05, which means that the interfacial thickness is 5% of the droplet radius.

An important dimensionless parameter—the magnetic bond number Bo_m is utilized to demonstrate the ratio between magnetic stress tensor to surface stress tensor and to illustrate the ferrodroplet deformation under the magnetic strength over the surface [30]:

$$Bo_m = \frac{\mu_0 (H_0)^2}{\sigma \kappa_0} \sim \frac{\nabla \cdot \boldsymbol{\tau}_m}{G \nabla \phi},\tag{26}$$

where μ_0 is the permeability in vacuum, H_0 is the externally applied magnetic strength, and κ_0 is the curvature of the initial un-deformed droplet of radius R_0 with the relationship $\kappa_0 = 2/R_0$ [30]. When the bond number is large enough, the

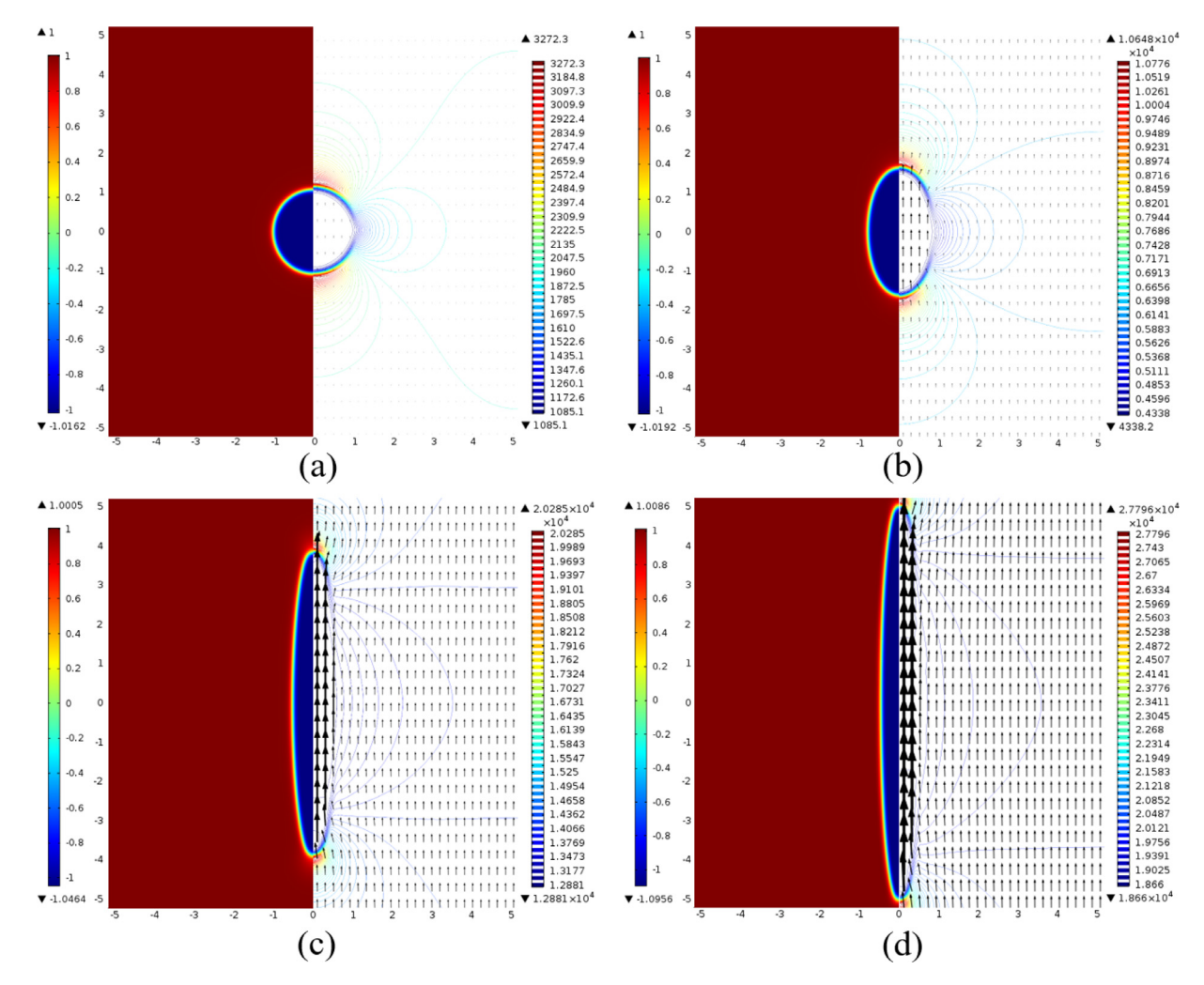


Fig. 5. The 2D cross-section shapes of ferrodroplet(left) and the magnetic field distributions(right) in the final quasi-equilibrium state T=0.1 s with four different values of magnetic bond number: (a) $Bo_m=0.1$, (b) $Bo_m=1$, (c) $Bo_m=5$ and (d) $Bo_m=10$ with the magnetic susceptibility is defined as $\chi_f=3$. The contour distributions shown are for the magnetic field strength \boldsymbol{H} and the arrows indicate the strength and the directions of magnetic induction \boldsymbol{B} .

magnetic effect will dominate over the surface tension effect. On the other hand, when $Bo_m \to 0$, the magnetic effect could be neglected compared with the surface tension.

The Reynolds number for the transient flow induced by the external magnetic fields in the dynamic ferrodroplet deformation process is expressed as:

$$Re = \frac{\rho \mu_0 (H_0)^2 (R_0)^2}{\eta^2} \tag{27}$$

which represents ratio of the inertia multiplied by the magnetic force to the square of the viscous drag. It means that higher magnetic field leads to stronger induced transient flow. This dimensionless number will be discussed in our numerical results in relation to the dynamic transition in the deformation process under applied uniform magnetic fields.

4.3. Shape of ferrodroplet at equilibrium

To validate the two Rosensweig models in Sections 2 and 3, the numerical results will be compared with the well-known analytical solutions which are derived theoretically to predict the equilibrium shape of the ellipsoidal ferrodrop at low or moderate deformations. Based on the assumptions of the ellipsoidal shape of ferrodroplet and the uniform magnetic strength inside the ferrodrop [30], the following relationship between the aspect ratio $\gamma = b/a$ and the magnetic bond number Bo_m holds:

$$Bo_m = \left[\frac{1}{\chi} + k\right]^2 \left(\frac{b}{a}\right)^{\frac{1}{3}} \left(2 \cdot \frac{b}{a} - \left(\frac{b}{a}\right)^{-2} - 1\right) \tag{28}$$

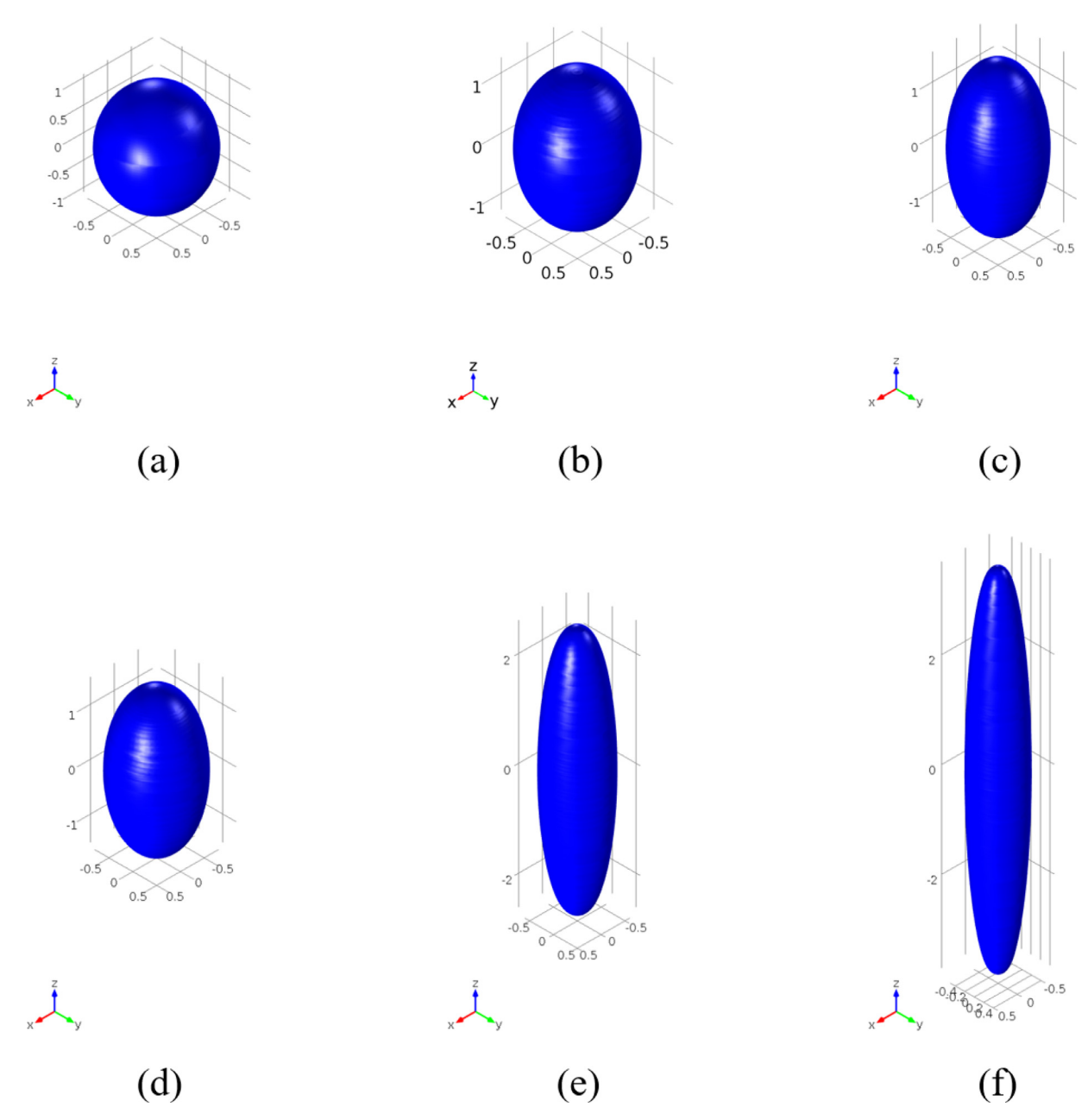


Fig. 6. 3D results of ferrodroplet deformation at the equilibrium state for the magnetic bond number $Bo_m = 1$ with the magnetic susceptibility (a) $\chi_f = 1$, (b) $\chi_f = 2$ and (c) $\chi_f = 3$ and for the magnetic bond number $Bo_m = 5$ with the magnetic susceptibility (d) $\chi_f = 1$, (e) $\chi_f = 2$ and (f) $\chi_f = 3$.

where $\chi = (\mu_f - \mu_n)/\mu_n$ is the fixed magnetic susceptibility, a and b are the half of minor axis and the half of major axis of the deformed ellipsoidal ferrodrop, respectively. The parameter k is the demagnetizing factor:

$$k = \left(\frac{1 - E^2}{2E^3}\right) \left(\ln\frac{1 + E}{1 - E} - 2E\right) \tag{29}$$

where $E = \sqrt{1 - a^2/b^2}$ is the eccentricity. The relation between the aspect ratio $\gamma = b/a$ at equilibrium and the magnetic bond number Bo_m is depicted in Fig. 2 with respect to different magnetic susceptibility of ferrofluid χ_f .

4.4. Fluid properties and numerical implementations

For the ferrofluid we choose EMG707 with the density $\rho_f = 1100(kg/m^3)$, the viscosity $\eta_f = 0.005(Pa*s)$, the magnetic permeability $\mu_f = \mu_0(1 + \chi_f)$, and the magnetic susceptibility $\chi_f = 1.51$. For the non-magnetic medium we choose Silicone

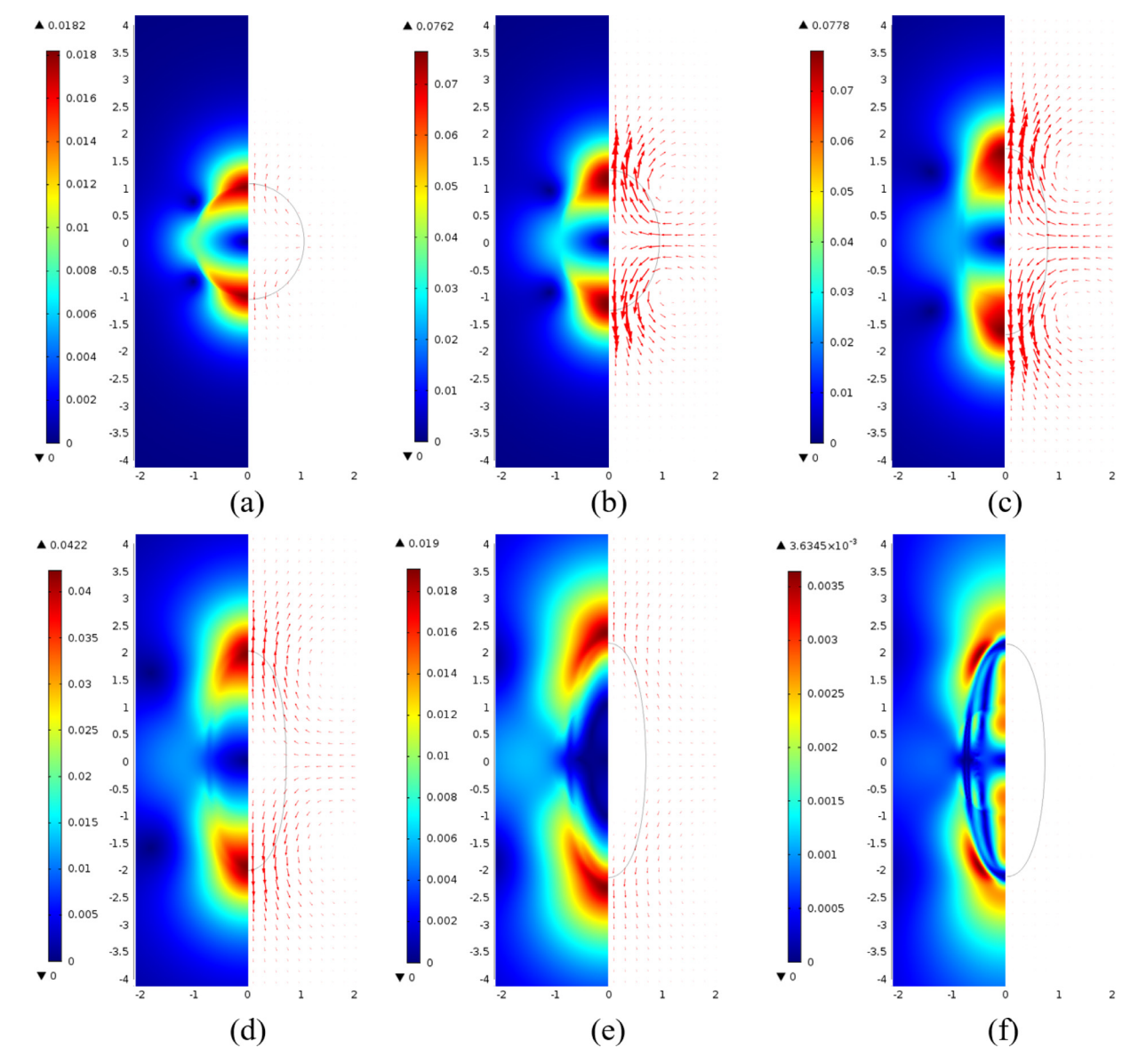


Fig. 7. The velocity of flow at six different time instances using the phase field approach (a) t = 0.01 s, (b) t = 0.01 s, (c) t = 0.02 s, (d) t = 0.02 s, (e) t = 0.03 s, (f) t = 0.05 s. The magnetic bond number is $Bo_m = 5$ and the magnetic susceptibility of ferrodroplet is chosen as $\chi_f = 1.51$ for the EMG707.

oil with the density $\rho_n = 960(kg/m^3)$, the viscosity $\eta_n = 0.05(Pa*s)$, the magnetic permeability $\mu_n = \mu_0(1 + \chi_n)$, and the magnetic susceptibility $\chi_n = 0$. The value of natural magnetic permeability in vacuum is $\mu_0 = 1.257 \times 10^{-6} (N/A^2)$. The surface tension coefficient between the two immiscible phases is chosen to be about $\sigma = 0.025(N/m)$ [109,110].

In phase field models the phenomenological mobility in the Cahn–Hilliard equation could be determined by the criterion of characteristic mobility $M_c = \chi_{mo} \varepsilon^2$ [104]. According to Eq. (6) in the previous section, the chemical potential is linearly proportional to the surface tension coefficient σ . In order to keep the diffusion term in the Cahn–Hilliard equation at a reasonable level, the mobility (M) is chosen to be inversely proportional to the surface tension coefficient (σ) in the chemical potential G when the interfacial thickness ε is kept as a constant (Cn=0.05). In Silicone oil – EMG707 two-phase system, the surface tension coefficient is five times of that value in water – mineral oil system [104], which causes that the characteristic mobility in Silicone oil – EMG707 system is one fifth of that in water-mineral oil system by keeping the constant interfacial width. Together with $\varepsilon=0.05R_0=0.05\times 1$ mm = 0.05 mm, we obtain the value of the characteristic mobility $\chi_{mo}=0.201(m\cdot s/kg)$ in this two-phase system.

We choose the 2D axisymmetric coordinate (cylindrical coordinates $\Omega(r,z)$) to simulate the ferrodroplet deformation by using a standard finite elements package — COMSOL Multiphysics. In general numerical implementations, the triangle mesh cells are used in the 2D axisymmetric system with the size of $0.025R_0$ and the total number of the mesh cells is about

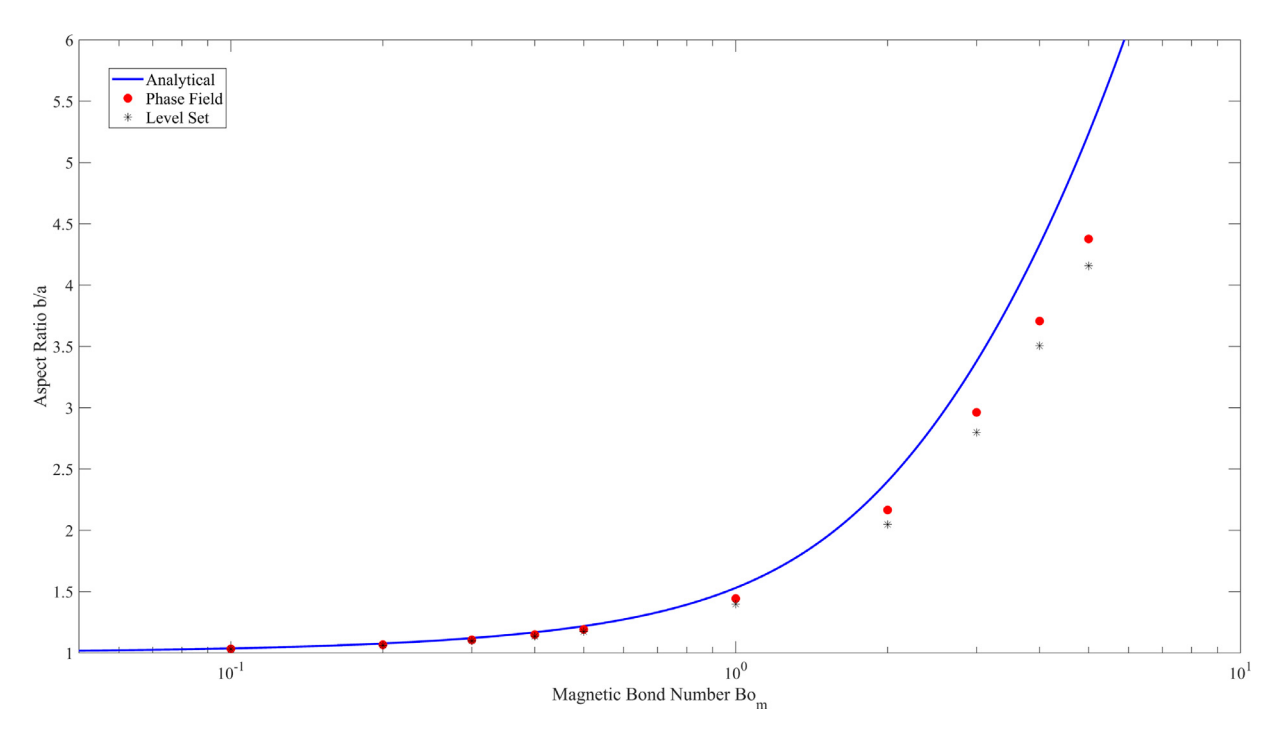


Fig. 8. The comparison between the numerical results of the phase field approach/modified level set approach and the analytical results for the aspect ratio at T = 0.1s with respect to different values of magnetic bond number Bo_m . The magnetic susceptibility $\chi = 1.51$ is chosen for the Silicon-EMG707 system.

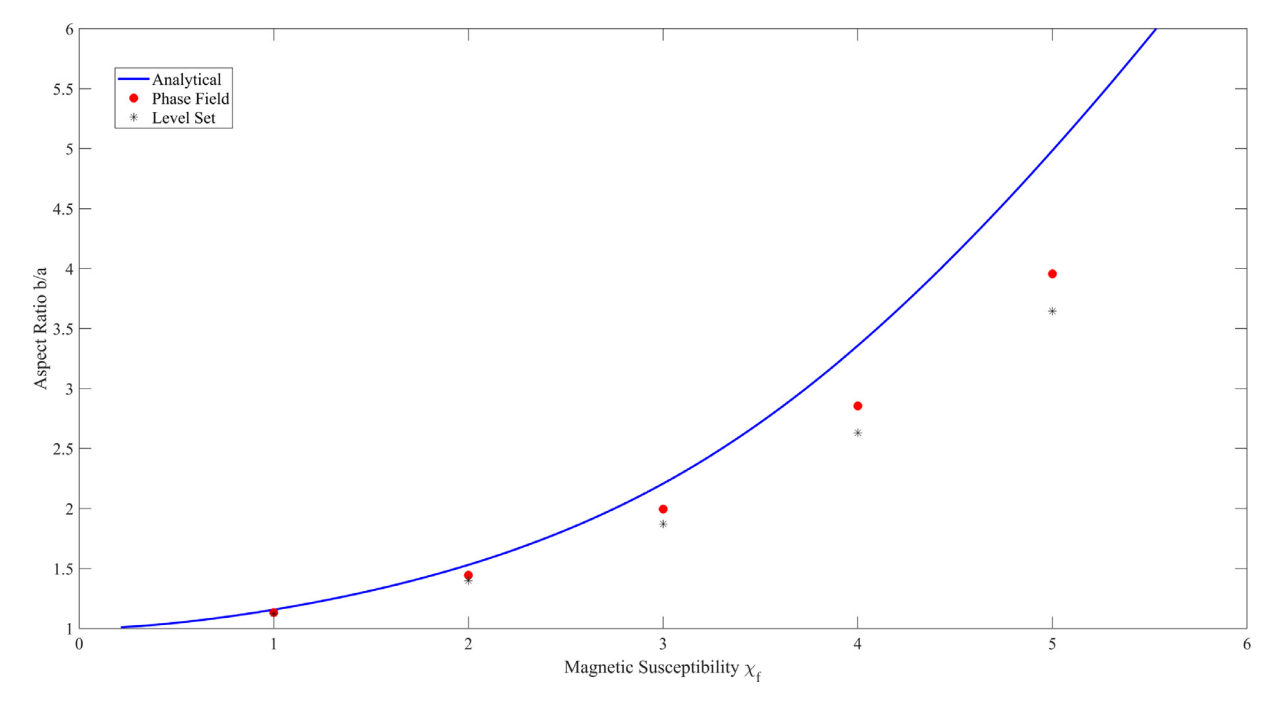


Fig. 9. The comparison between the numerical results of the phase field approach/modified level set approach and the analytical solutions for aspect ratio at T = 0.1s with respect to different values of the magnetic susceptibility. The magnetic bond number is $Bo_m = 1$.

 $N_{mesh}=24,000$ in the whole domain(Ω). In the finite element algorithms, linear finite elements are chosen to approximate the pressure while quadratic finite elements are chosen to predict the other unknowns in the governing equations. The total computational time span is T=0.1s with the small time step $\delta t=10^{-4}$ s. Therefore the computational cost in both two numerical approaches are nearly the same. Furthermore, when using open-source packages instead of COMSOL for simulation, pre-conditioners can be considered for solving the system more efficiently [111–116]. In the following section

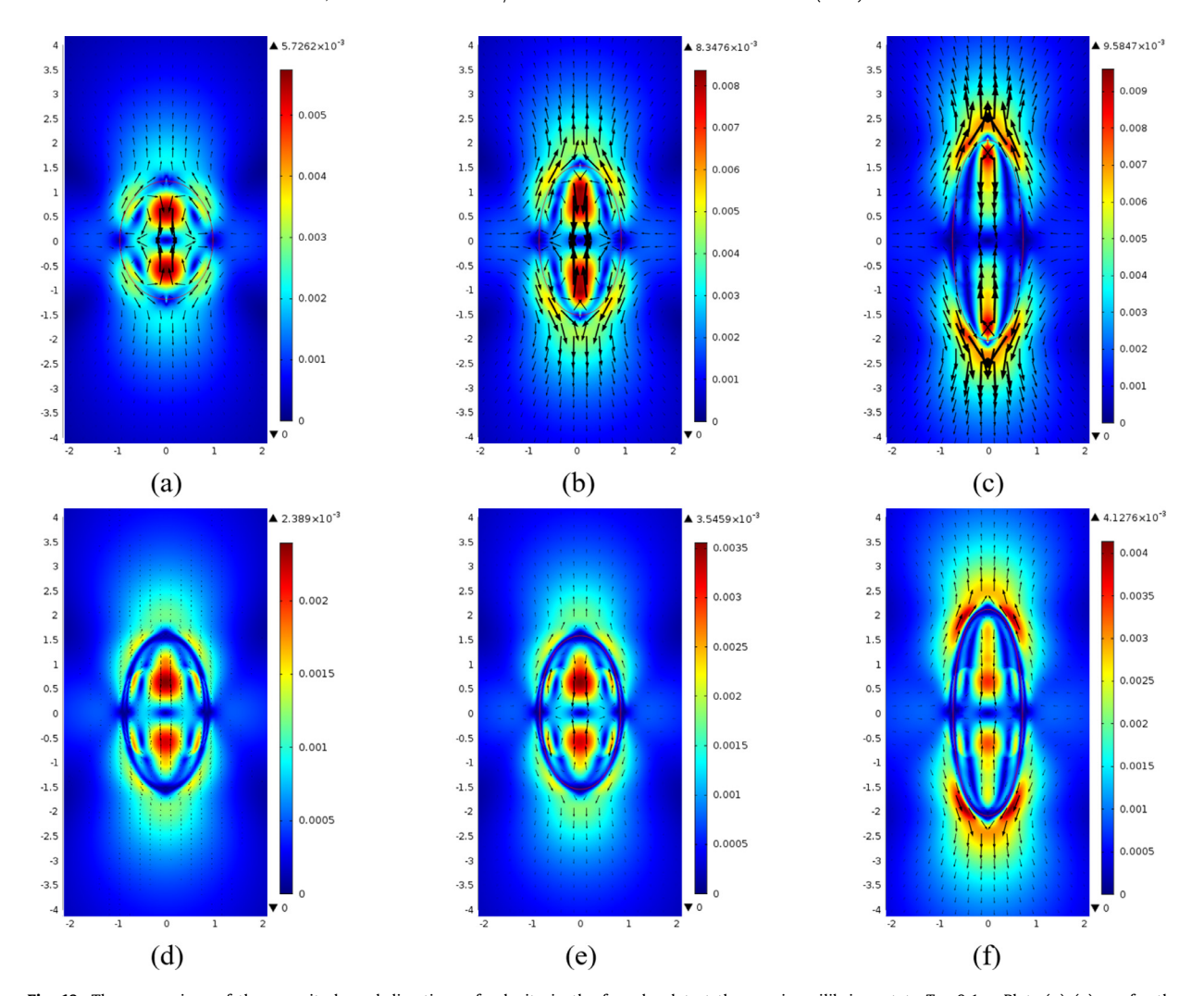


Fig. 10. The comparison of the magnitude and directions of velocity in the ferrodroplet at the quasi-equilibrium state T = 0.1 s. Plots (a)–(c) are for the level set model and plots (d)–(f) are for the phase field model with different magnetic bond numbers $Bo_m = 2, 5, 10$. The magnetic susceptibility is chosen as $\chi_f = 1$.

we will discuss about the results of numerical experiments in details to validate the two models in Sections 2 and 3 and illustrate their features.

5. Numerical results and discussions

5.1. The numerical results of the Rosensweig model by the phase field approach

In this section we compare our numerical results of phase field approach and the analytical solutions to validate our numerical model. The characteristic mobility (M_c) is utilized in the phase field approach for the Silicon-EMG707 system [104].

We first utilize the Rosensweig model with phase field approach to simulate the ferrodroplet deformation and compare the numerical results with the well-known analytical solutions at the quasi-equilibrium state. Fig. 3 demonstrates this comparison by using the relationship between the aspect ratio $\gamma = b/a$ and the magnetic bond number Bo_m at the equilibrium state with four different values of magnetic susceptibility ($\chi_f = 1, \chi_f = 1.51, \chi_f = 2, \chi_f = 3$). In the real Silicone-EMG707 system, the magnetic susceptibility is about $\chi_f = 1.51$. It is observed that the numerical results well match the analytical solutions for relatively small values of Bo_m . When the magnetic bond number Bo_m increases, the numerical results begin to deviate from the analytical solutions. It can also be seen that the larger magnetic susceptibility χ_f leads to larger discrepency between the numerical results and the analytical solutions. Another interesting observation is that the numerical predictions are always smaller than the corresponding analytical solutions.

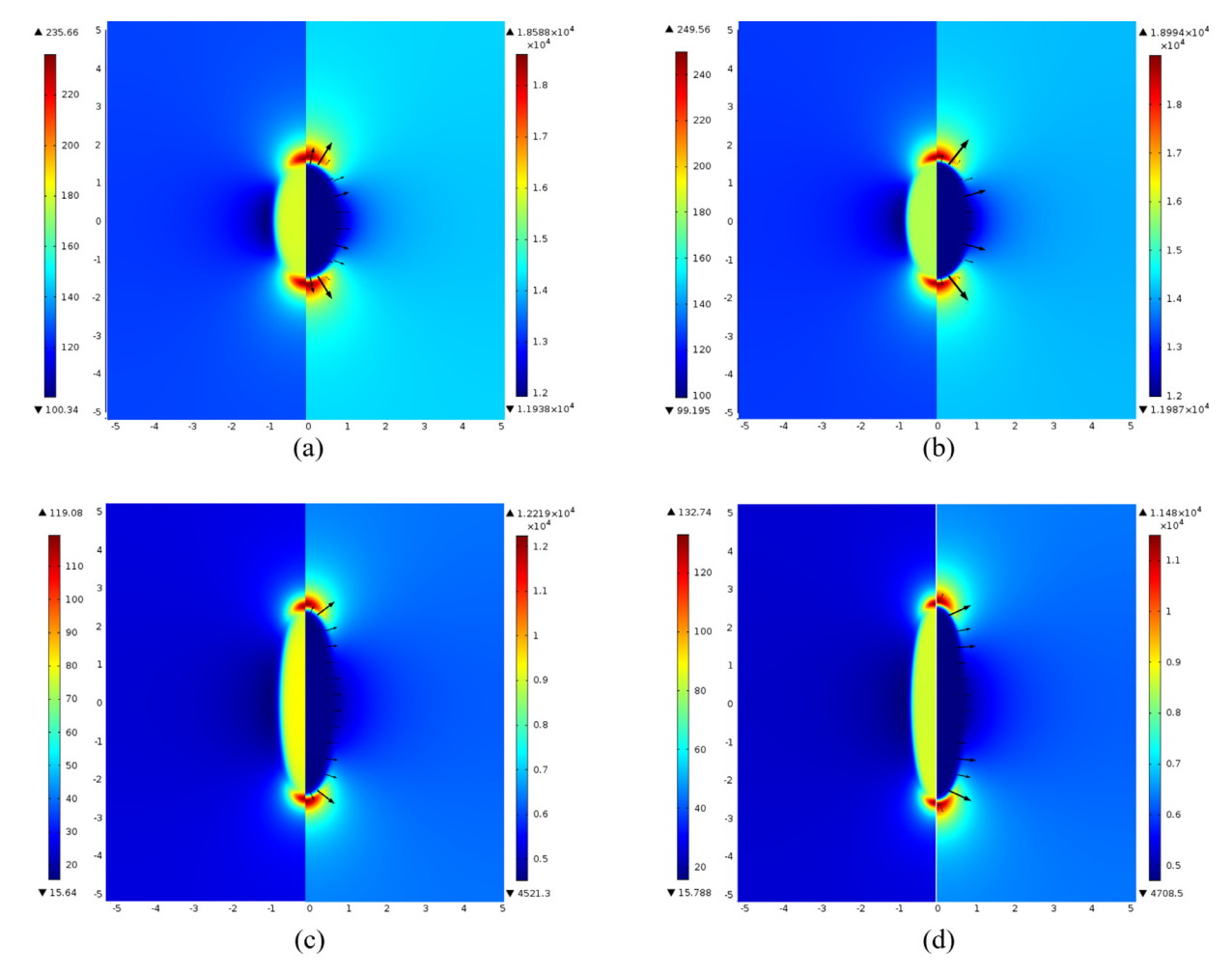


Fig. 11. The magnetic energy density distributions (left parts) and the magnetic field strength (right parts) at the quasi-equilibrium state T = 0.1 s. Plots (a)(c) are for the level set model and plots (b)(d) are for the phase field model with different magnetic bond numbers. $Bo_m = 5$ and $\chi_f = 1$ are chosen for plots (a)(b) and $Bo_m = 1$ and $\chi_f = 5$ are chosen for plots (c)(d). The arrows show the directions and magnitudes of magnetic force (F_m) along the two-phase interface.

On the other hand, the analytical solution is theoretically derived based on the hypothesis that the shape of the droplet is ellipsoid and the external magnetic field is uniform. When Bo_m and χ_f are large enough, the shape of the ferro-droplet deviates from the ellipsoid, especially at large deformation, in which the normal stress over the entire interface may not be satisfied. Hence the deviation between the analytical solution and the numerical solution becomes obvious as Bo_m increases.

Fig. 4 demonstrates the shapes (left parts) and magnetic field distributions (right parts) with the four different values of magnetic bond number by setting the magnetic susceptibility as $\chi_f = 1.51$ to reflect the real Silicone-EMG707 system. It can be observed that the deformed shape is elongated along the direction of the external magnetic fields and the shape of the ferrodroplet tends to be more ellipsoidal with the increasing the magnetic strength. The left parts indicate that the numerical undershoots and overshoots of the phase function ϕ are well controlled in a small magnitude and only slightly changed when the magnetic field becomes strong enough. From the right parts we can observe that both the magnetic field strength (in contours) and the magnetic induction(in arrows) are nearly uniform both inside the droplet and far from the droplet, which matches another assumption of the analytical solutions [30].

Moreover, Fig. 5 demonstrates the same type of results as in Fig. 4, by setting the magnetic susceptibility as $\chi_f = 3$. The results show that the larger magnetic susceptibility leads to larger deformation with the corresponding magnetic bond numbers. This validates what we observed in Fig. 3.

Fig. 6 illustrates the 3D shapes of the ferrodroplet at the quasi-equilibrium state (T = 0.1 s). From this 3D figure it is observed that the shapes of the deformed ferrodroplet are generally ellipsoidal and are elongated along the directions of the external applied magnetic fields with various magnetic bond number Bo_m and magnetic susceptibility χ_f , which shows the

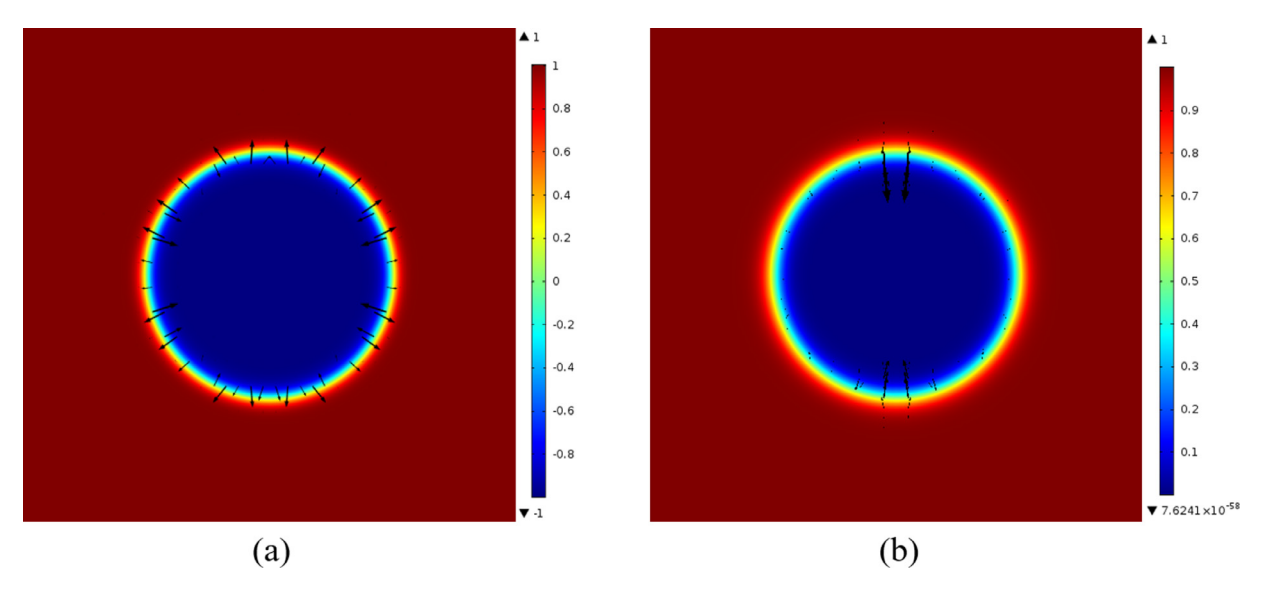


Fig. 12. The spurious flow near the interface in the phase field approach (a) and the modified level set approach (b) at the beginning of the numerical simulation (T = 0.001 s). The length of the arrows represents the magnitude of the spurious velocity and the directions of the arrows indicate the direction of spurious flow. For the diffuse interface model: Cn = 0.05 and for the sharp interface model: $Cn = 0.05R_0$.

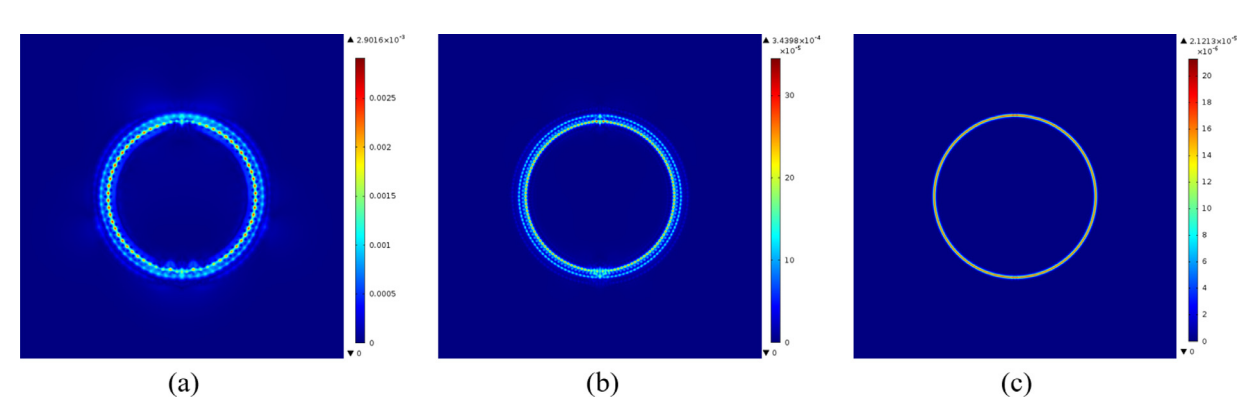


Fig. 13. The spurious flow near the interface using the phase field approach at the beginning of the numerical simulation (t = 0.001 s). This group demonstrates the magnitude of spurious flow with the decreasing mesh size 0.1 mm (a), 0.05 mm (b), and 0.025 mm (c). The Cahn number representing the thickness of diffuse interface is fixed as: Cn = 0.05.

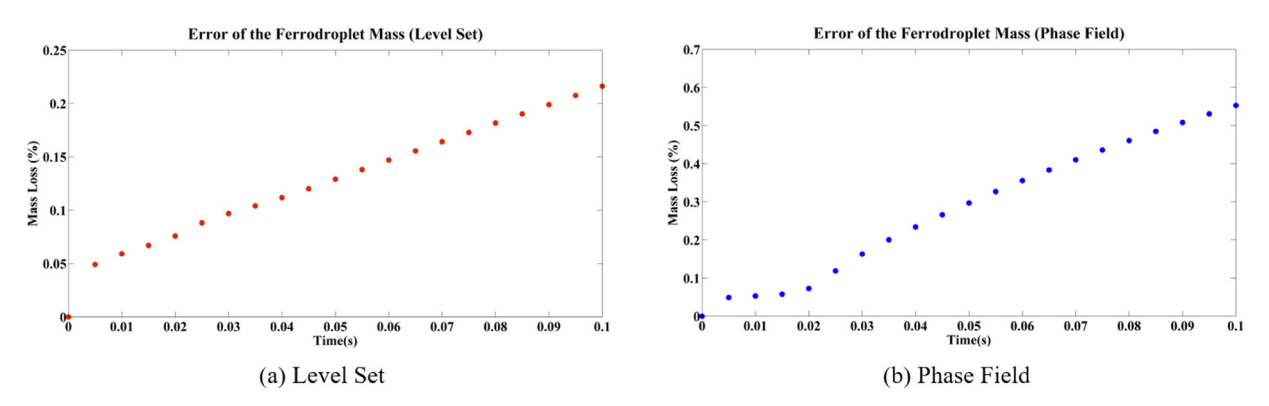


Fig. 14. The evolution of the numerical error of mass in ferrodroplet both in (a) the modified level set approach and (b) the phase field approach in the whole time span T=0–0.1 s. The magnetic bond number is $Bo_m=1$ and the magnetic susceptibility $\chi_f=1.51$ in the two-phase Silicon-EMG707 system.

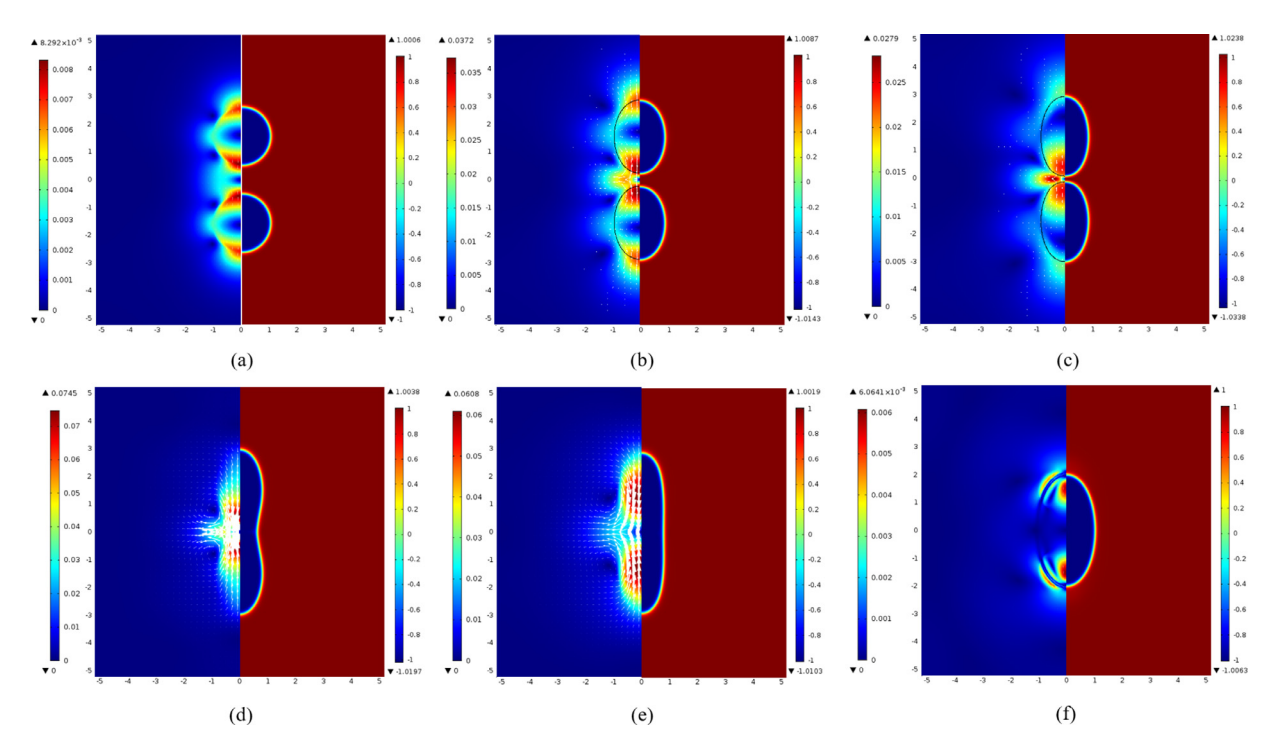


Fig. 15. The coalescence of two ferrodroplets using the phase field approach: the velocity magnitude and direction(left) and the phase variable(right) are shown in color legends. The external magnetic field strength is $Bo_m = 2$. The evolution time steps in the process are: (a) t = 0.01 s, (b) t = 0.02 s, (c) t = 0.025 s, (d) t = 0.035 s, (e) t = 0.04 s and (f) t = 0.1 s. The two phase fluid system is Silicon - EMG707.

agreement between the analytical solutions and the diffuse interface model. It is clearly seen that the deformation in plots (d)-(f) is larger than that in plots (a)-(c) with the increasing magnetic bond number. This indicates that the deformation is more sensitive to the magnetic susceptibility at relative large magnetic bond number Bo_m .

Fig. 7 shows the velocity distributions in the dynamic deformation process of the model from t=0.01 s to t=0.05 s with the magnetic bond number $Bo_m=5$. This dynamic transition process could be described by the transition Reynolds number $Re=\frac{\rho\mu_0(H_0)^2(R_0)^2}{\eta^2}$ which represents the inertia multiplying the magnetic stress over the viscosity. In our work the magnetic bond number Bo_m is ranging from 0.1 to 10, the corresponding transient Reynolds number Re ranges from 5 to 500, which means the induced flow in the dynamic ferrodroplet deformation process belongs to the typical laminar flow($Re \ll 2000$). In Fig. 7 the Reynolds number is about Re=250 corresponding to $Bo_m=5$. At the beginning, the flow velocity increases with the step function $\beta(t)$ (from t=0 s to t=0.02 s). Then the ferrodroplet comes to a slight oscillation state with minor flows around the interface near the top and bottom of the droplet. After t=0.05 s the ferrodroplet tends to reach the quasi-equilibrium state.

5.2. Comparison between the results of the phase field approach and the modified level set approach

In this subsection the numerical results in both phase field approach and modified level set approach are compared with the analytical solutions. The characteristic mobility (M_c) is utilized in the phase field approach for the Silicon-EMG707 system [104].

Fig. 8 shows the comparison between the numerical results of phase field approach and modified level set approach with analytical solutions at the quasi-equilibrium state (T=0.1 s) for the Silicon-EMG707 system (with magnetic susceptibility $\chi_f=1.51$). The results of both phase field approach and modified level set approach well match the analytical solutions when the magnetic bond number is small enough ($Bo_m \le 1$), however, as Bo_m grows the deviations between numerical results and the analytical solutions increases correspondingly. On the other hand, Fig. 9 shows the similar comparison between the numerical results of the two numerical methods and the analytical solutions with respect to the variations of the magnetic susceptibility (χ_f from 1 to 5). According to these two figures it can be observed that when Bo_m or χ_f grows, the error between the numerical and analytical results increases and we can also observe that the results of phase field approach are more accurate than the results of modified level set approach for relative large values of Bo_m and χ_f by using the characteristic mobility (M_c) in the diffuse interface model using Cahn–Hilliard equation. In other words we can find that the phase field model could better reflect the ellipsoidal shape of ferrodroplet in large deformation at large uniform magnetic field.

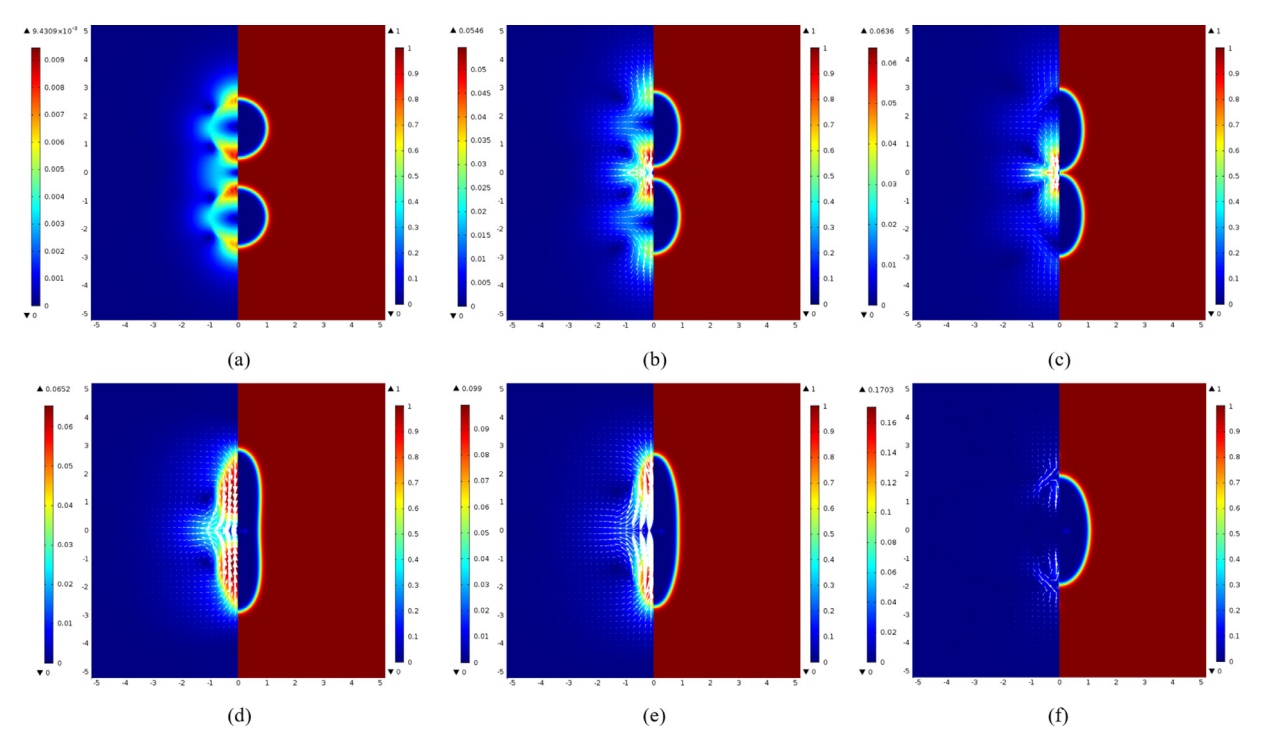


Fig. 16. The coalescence of two ferrodroplets using the modified level set approach: the velocity magnitude and direction(left) and the level set variable(right) are shown in color legends. The external magnetic field strength is $Bo_m = 2$. The evolution time steps in the process are: (a) t = 0.01 s, (b) t = 0.02 s, (c) t = 0.025 s, (d) t = 0.035 s, (e) t = 0.04 s and (f) t = 0.1 s. The two phase fluid system is Silicon - EMG707.

The comparison between the phase field approach and the modified level set approach for the velocity is shown in Fig. 10. It could be observed that there are four velocity vortexes symmetrically distributed inside the ferrodroplet. The instability of the velocity field increases with the strength of magnetic field ($Bo_m = 2 \rightarrow 10$) for both models. And the instability of the velocity field of the modified level set approach is higher than that of the phase field approach.

Fig. 11 illustrates the magnetic energy density distributions ($e_m = |\frac{1}{2}\mu H^2|$ in the left parts) and the magnetic field strength (H in the right parts) for both the phase field approach and the modified level set approach. We can see that the maximum values of the magnetic density and the magnetic strength are found at the top and bottom of the ferrodroplet for the both two kinds of models. The minimum values of magnetic energy density is located outside the ferrodroplet, while the minimum values of magnetic field strength is inside the ferrodroplet. Both the magnetic energy density and the magnetic strength are uniform inside the ferrodroplet, which illustrates the agreement between the analytical solutions and the numerical models in both two methods. The deformation of the sharp interface model is slightly weaker than that of the diffuse interface model. The directions of the magnetic force are the same as the outward normal vector perpendicular to the two-phase interface.

5.3. Spurious phenomenon and the conservation of mass in ferrodroplet

The spurious flow on the interface between the two immiscible phases is a common numerical artifact by performing the capillary stress on the interface as a volume force in Navier–Stokes equation [117,118]. The magnitude of spurious flow is determined by the density ratio of the two phases, the surface tension coefficient and the size of mesh cells around the interface. It is reported that the strong surface tension will lead to aggravate the spurious flow currents and cause instability at the interface. Also large density ratio will cause the spurious flow and it is difficult to be eliminated. If the mesh cells are too coarse, numerical errors will lead to large instability in the interface region. In our cases, the surface tension coefficient $\sigma = 0.025 \text{ N/m}$ is not large enough to cause large spurious currents and the density ratio is only $\zeta = \frac{\rho_n}{\rho_f} \approx 1.15$. We choose the mesh cells to be half of the interfacial thickness $\delta h = 0.5\varepsilon = 0.5\varepsilon$ so that it is small enough to weaken the spurious flow caused by numerical errors.

In Fig. 12 the spurious flow is found at the beginning (at T = 0.001 s) of both the phase field approach and modified level set approach when the magnetic field is weak according to the step function configuration at the bottom surface. The magnitude of spurious flow is nearly uniform at the diffuse interface in the phase field model. On the other hand, in the level set model, the spurious flow near the centerline(r = 0) is relatively larger than the others around the interface. In the phase field approach the radius of the ferrodroplet decreases from 1mm to 0.996mm from the initial time to 0.001 s, which

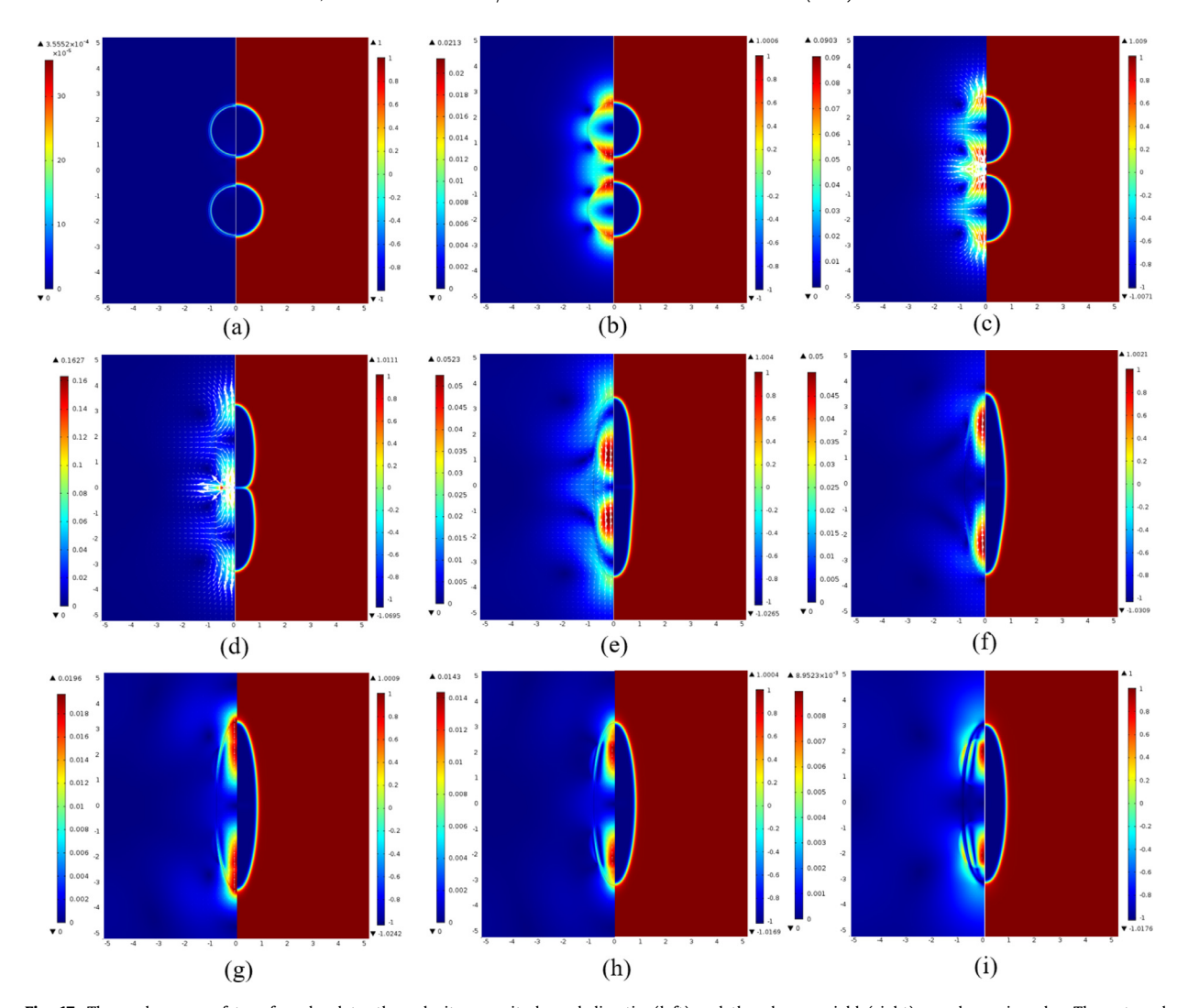


Fig. 17. The coalescence of two ferrodroplets: the velocity magnitude and direction(left) and the phase variable(right) are shown in color. The external magnetic field strength is $Bo_m = 5$. The evolution time steps in the process are: (a) t = 0.001 s, (b) t = 0.01 s, (c) t = 0.015 s, (d) t = 0.02 s, (e) t = 0.025 s, (f) t = 0.03 s, (g) t = 0.04, (h) t = 0.05 s and (i) t = 0.1 s. The two phase fluid system is Silicon – EMG707.

demonstrates the uniform diffusive effect around the diffuse interface for the phase field approach. When the step function increases with time, the spurious currents are weakened to be negligible after t = 0.005 s in both two numerical methods.

Furthermore, Fig. 13 demonstrates the magnitude of the spurious flow occurring at the beginning time (t = 0.001 s) when the phase field approach is used with the decreasing mesh sizes 0.1 mm, 0.05 mm and 0.025 mm, respectively. It is clearly shown that the spurious flow is significantly weakened during the mesh refinement.

It is noticed that the spurious flow could be removed by the pressure correction method in the two-phase phase field model [119]. We believe this kind of phase field model could be utilized in the two-phase ferrofluid problems and in future we may upgrade the phase field model with this new method for more accurate numerical solutions.

The mass conservation in the two-phase fluid flow simulations is a basic and crucial criterion for justifying the correctness of the numerical results. In our study, we examine the evolution of mass conservation with time for the ferrodroplet to justify mass conservation of the two numerical approaches. The mass loss during the time evolution process is defined as:

$$err_m = \frac{\mid M_0 - M_t \mid}{M_0},\tag{30}$$

where M_0 is the initial total mass for the ferrodroplet and M_t is the total mass for the ferrodroplet with time variations. Fig. 14 indicates the evolution of numerical error of mass in ferrodroplet both in the modified level set approach(the sharp interface) and the phase field approach(the diffuse interface). The results show that both the errors in two approaches are smaller than 0.6% in the deformation. We can also observe that the mass loss in the phase field approach is relative larger

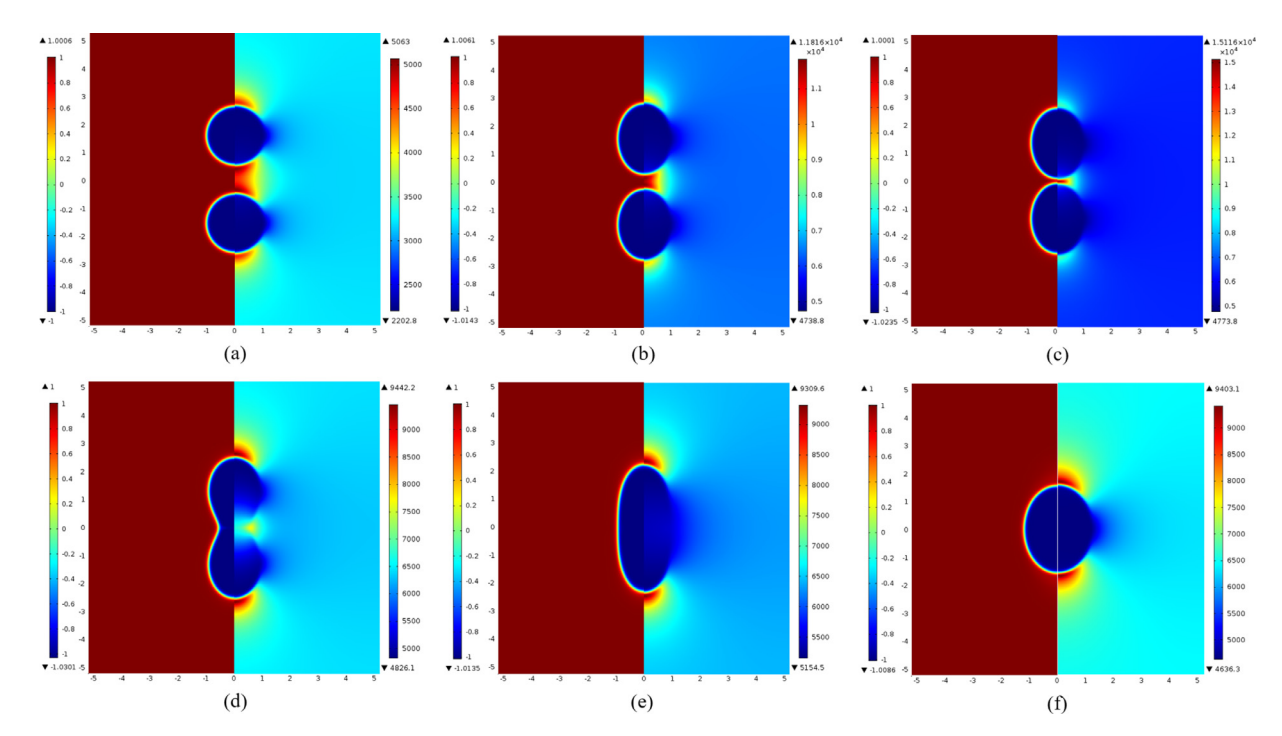


Fig. 18. The coalescence of two ferrodroplets in the phase field approach: The phase variable(left) and the magnetic field strength(right) are shown in color. The evolution time steps in the process are: (a) t = 0.01 s, (b) t = 0.03 s, (c) t = 0.06 s, (d) t = 0.07 s, (e) t = 0.08 s and (f) t = 0.1 s. The external magnetic field strength is $Bo_m = 1$. The two phase fluid system is Silicon – EMG707.

than it in the modified level set approach, which demonstrates that the mass loss in the diffuse interface method is relative larger than the level set. However, in total the mass loss in the simulations are very small in both two approaches and the mass conservation could be satisfied by the mass examination.

5.4. Coalescence of two ferrodroplets in a uniform magnetic field

In this section we simulate the coalescence phenomenon of two ferrodroplets immersed in the non-magnetic viscous fluid under uniform magnetic fields by using the phase field method and the modified level set method. Both of the paired ferrodroplets have the radius R = 1 mm. The upper ferrodroplet is centered at S1 = (0, 1.5)(mm) and the lower ferrodroplet is centered at S2 = (0, -1.5)(mm). Other parameters are the same as what we discussed in Section 4.4.

We utilize external uniform magnetic fields to elongate two ferrodroplets for the process of coalescence. When the two droplets are slender enough (the aspect ratio is large enough), the two elongated ferrodroplets touch with each other and combine together to form a new larger ferrodroplet. For this purpose, the magnetic bond number Bo_m should be chosen as the large enough values. The results of Section 5.2 indicate that the two ferrodroplets could touch with each other when $Bo_m > 1.8$ in the Silicon-EMG707 system. Figs. 15 and 16 demonstrate the merging procedure of the two ferrodroplets with the magnetic bond number $Bo_m = 2$ by utilizing the phase field method and the modified level set method, respevtively. We can observe that at the beginning the two droplets deform as what occurs in our previous study. As the two ferrodroplets approach to each other, the magnitude of flow velocity between them increases significantly. Then the two ferrodroplets touch with each other and evolve into a larger single ferrodroplet. After the single larger ferrodroplet is generated, the symmetric velocity eddies at the center still exist since the inertia phenomenon takes effect on the interface evolution. Then the magnitude of flow velocity gradually decays due to the fluid viscosity and the elongated single large ferrodroplet finally reaches a stable elliptical shape. Furthermore, the same coalescence phenomenon is also observed with refined meshes.

In Fig. 17 the merging process is demonstrated using the phase field approach with the larger magnetic bond number $Bo_m = 5$. Compared with the coalescence with respect to the magnetic strength $Bo_m = 2$, the two ferrodroplets have larger deformation and merge with each other much faster as expected.

Recently an interesting phenomenon was observed in numerical studies [62]: even when the external magnetic field is not strong enough to directly elongate the two ferrdroplets to touch with each other, the two ferrdroplets may be still attracted to each other to combine and form a larger ferrdroplet. In our numerical simulation with $Bo_m = 1$, similar phenomenon is also observed by using both the two numerical approaches. In Fig. 18, the results of the phase field approach are presented. At the beginning the two ferrodroplets are elongated but do not touch with each other. However, the two drops gradually move to each other and meet around t = 0.065 s. Then the two small ferrodroplets begin to merge with

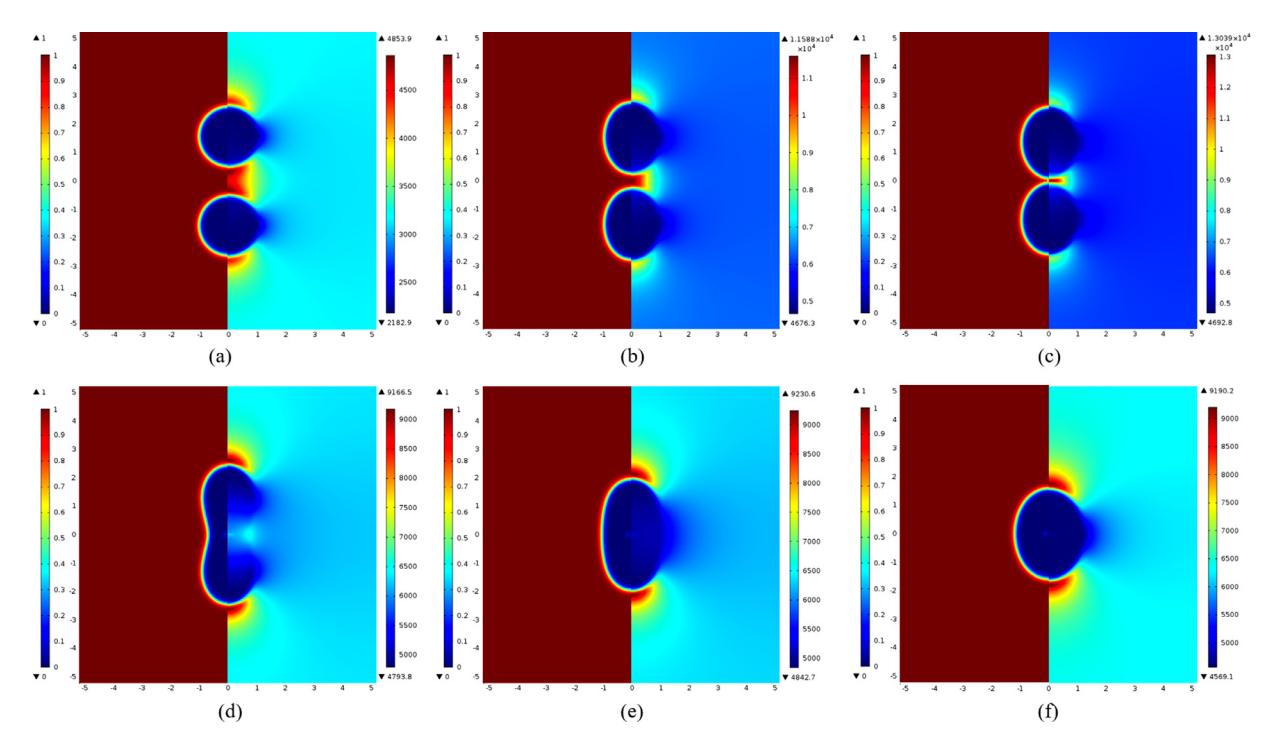


Fig. 19. The coalescence of two ferrodroplets in the modified level set approach: The level set variable(left) and the magnetic field strength(right) are shown in color. The evolution time steps in the process are: (a) t = 0.01 s, (b) t = 0.03 s, (c) t = 0.05 s, (d) t = 0.06 s, (e) t = 0.07 s and (f) t = 0.1 s. The external magnetic field strength is $Bo_m = 1$. The two phase fluid system is Silicon – EMG707.

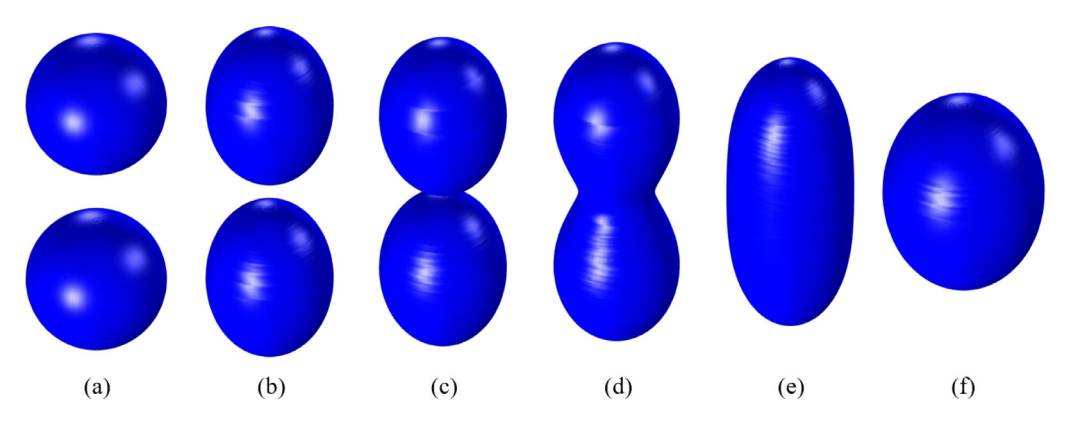


Fig. 20. The coalescence of two ferrodroplets in 3D: The evolution time steps in the process are: (a) t = 0.01 s, (b) t = 0.03 s, (c) t = 0.06 s, (d) t = 0.07 s, (e) t = 0.08 s and (f) t = 0.1 s. The external magnetic field strength is $Bo_m = 1$. The two phase fluid system is Silicon – EMG707.

each other and a single larger ferrodroplet is generated with an elliptical shape at the equilibrium state. Before the two ferrodroplets touch with each other, the magnetic field between them is observed to be stronger than that of the rest of the domain, which can be one major reason to cause the mutual attraction between the two ferrodroplets. The same mutual attraction phenomenon is also observed by using the sharp interface method (the modified level set approach) in Fig. 19. The corresponding 3D illustration of this process is also shown in Fig. 20.

To further investigate on this phenomenon, we also study the effect of the magnetic susceptibility based on the same mesh and Bond number. The results are presented in Fig. 21. When magnetic susceptibility value is small ((a) $\chi_f = 0.5$), the two ferrodroplets could hardly move to each other and the coalescence phenomenon does not happen. However, the larger magnetic susceptibility ((b) $\chi_f = 1.51$ and (c) $\chi_f = 2.5$) values lead to the coalescence phenomenon. These results indicate that different magnetic susceptibility values may lead to different magnetic field strengths for attracting the two ferrodroplets, hence may or may not lead to the coalescence phenomenon, even based on the same mesh and Bond number. Since the mechanism of this phenomenon is not clear, more investigation for it can be interesting future works.

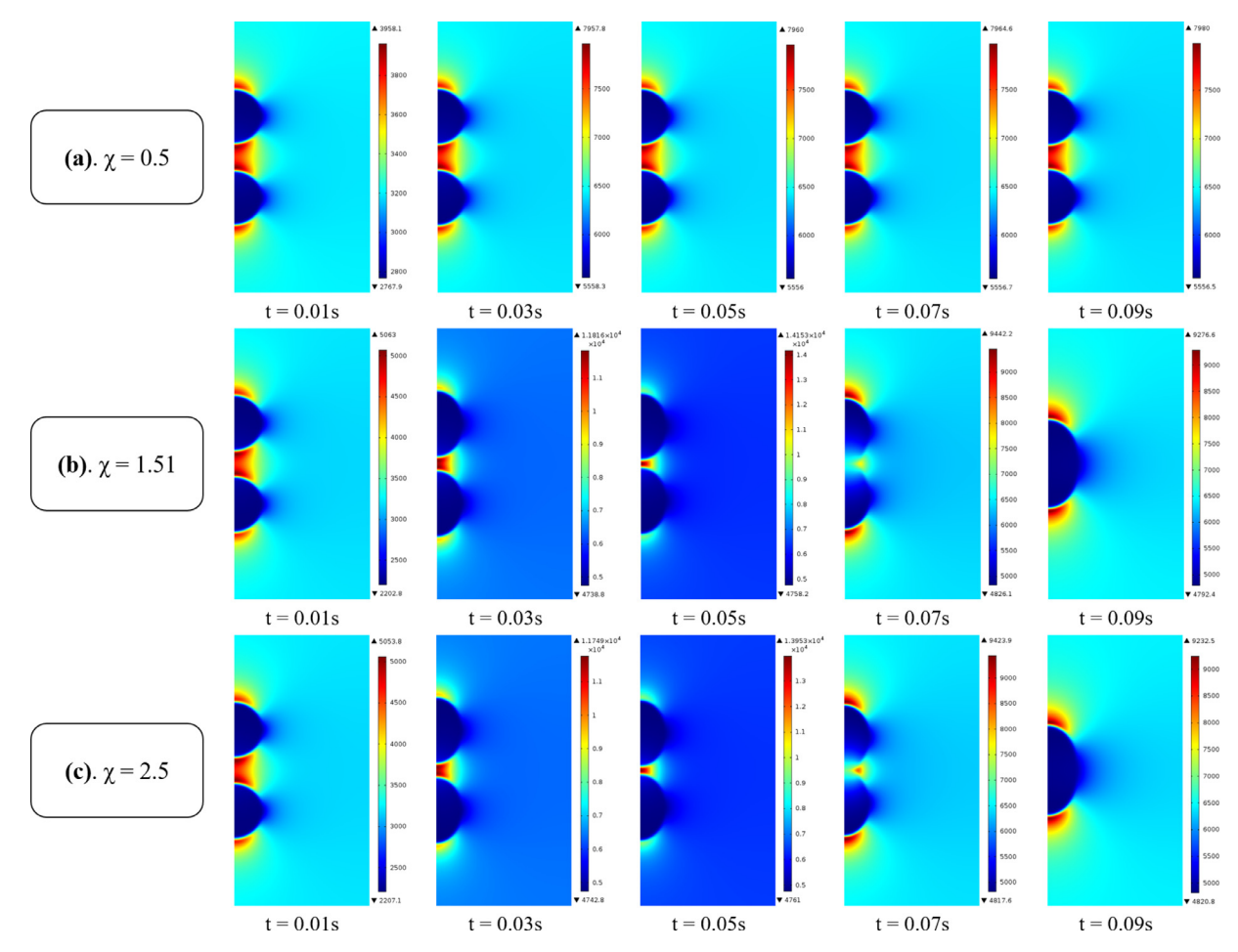


Fig. 21. The coalescence of two ferrodroplets in three different values of magnetic susceptibility: (a) $\chi_f = 0.5$, (b) $\chi_f = 1.51$ and (c) $\chi_f = 2.5$. The evolution time steps in the process are: t = 0.01 s, t = 0.03 s, t = 0.05 s, t = 0.07 s and t = 0.09 s. The external magnetic field strength is $Bo_m = 1$. The two phase fluid system is Silicon - EMG707.

6. Conclusions

In this paper we considered two multi-phase numerical Rosensweig models based on the phase field approach and a modified level set approach respectively to study the cases of one ferrodroplet deformation and two paired ferrodroplets merging process under external uniform magnetic fields. In particular, our models could deal with the general case of two-phase ferrofluid system with variable densities and viscosities. In the study of ferrodroplet deformation, the numerical results of both models were compared with the classic analytical solutions for the model validation. From the comparison it is shown that the numerical results of both models can reasonably approximate the analytical solutions at low or moderate magnetic bond number(Bo_m) and magnetic susceptibility(χ_f) while the phase field one is slightly closer to the analytical solution. According to the comparison between analytical and numerical solutions it is concluded that the phase field model is more accurate to present the ellipsoidal shape of ferrodroplet deformation than the modified level set model, especially in large deformations. This numerical observation may be applied to other topological phenomena such as electrocoalesence. Various interesting numerical and physical phenomenon, such as the effect of different parameters, the spurious phenomenon, the time evolution of mass conservation, and the coalescence between two paired ferrodroplets, were also studied by using the two proposed Rosensweig models.

Declaration of Competing Interest

The authors declare that they have no known competing financial interests or personal relationships that could have appeared to influence the work reported in this paper.

CRediT authorship contribution statement

Feng Bai: Methodology, Software, Writing - original draft. Daozhi Han: Conceptualization, Methodology, Writing - review & editing, Funding acquisition. Xiaoming He: Conceptualization, Methodology, Writing - review & editing, Supervision, Project administration, Funding acquisition. Xiaofeng Yang: Conceptualization, Software, Writing - review & editing, Funding acquisition.

Acknowledgments

This work is partially supported by NSF (DMS-1818642, DMS-1818783, DMS-1912715, DMS-1720212).

References

- [1] Rayleigh L. On the theory of surface forces II. Philos Mag 1892:33:209.
- [2] van der Waals J. The thermodynamic theory of capillarity under the hypothesis of a continuous density variation. J Stat Phys 1893;20:197–244.
- [3] Müller-Fischer N, Tobler P, Dressler M, Fischer P, Windhab EJ. Single bubble deformation and breakup in simple shear flow. Exp Fluids 2008;45(5):917-26.
- [4] Patlazhan S, Vagner S, Kravchenko I, Steady-state deformation behavior of confined composite droplets under shear flow. Phys Rev E 2015;91:063002.
- [5] Sherwood JD. The deformation of a fluid drop in an electric field: a slender-body analysis. J Phys A 1991;24(17):4047.
 [6] Salipante PF, Vlahovska PM. Electrohydrodynamics of drops in strong uniform dc electric fields. Phys Fluids 2010;22(11):112110.
- [7] Lanauze JA, Walker LM, Khair AS. Nonlinear electrohydrodynamics of slightly deformed oblate drops. J Fluid Mech 2015;774:245-66.
- [8] Nganguia H, Young YN, Layton AT, Lai MC, Hu WF. Electrohydrodynamics of a viscous drop with inertia. Phys Rev E 2016;93:053114.
- [9] Basaran OA, Wohlhuter FK. Effect of nonlinear polarization on shapes and stability of pendant and sessile drops in an electric (magnetic) field. I Fluid Mech 1992:244:1-16
- [10] Xi H-D, Guo W, Leniart M, Chong ZZ, Tan SH. Ac electric field induced droplet deformation in a microfluidic t-junction. Lab Chip 2016;16:2982-6.
- [11] Garton CG, Krasucki Z. Bubbles in insulating liquids: stability in an electric field. Proc R Soc Lond A 1964;280(1381):211-26.
- [12] Torza S, Cox RG, Mason SG. Electrohydrodynamic deformation and burst of liquid drops. Philos Trans Soc A 1971;269(1198):295-319.
- [13] Paknemat H, Pishevar AR, Pournaderi P. Numerical simulation of drop deformations and breakup modes caused by direct current electric fields. Phys Fluids 2012;24(10):102101.
- [14] Pillai R, Berry JD, Harvie DJE, Davidson MR. Electrolytic drops in an electric field: a numerical study of drop deformation and breakup. Phys Rev E 2015;92:13007.
- [15] Bacri JC, Salin D. Instability of ferrofluid magnetic drops under magnetic field. J Phys Lett 1982;43(17):649-54.
- [16] Bacri JC. Salin D. Massart R. Study of the deformation of ferrofluid droplets in a magnetic field. J Phys Lett 1982;43(6):179-84.
- [17] Bacri JC, Salin D. Dynamics of the shape transition of a magnetic ferrofluid drop. J Phys Lett 1983;44(11):415–20.
- [18] Rosensweig RE. Ferrohydrodynamics, 14. Cambridge University Press; 1985.
- [19] Rosensweig RE. Magnetic fluids. Annu Rev Fluid Mech 1987;19(1):437-61.
- [20] Rosensweig RE. Stress boundary-conditions in ferrohydrodynamics. Ind Eng Chem Res 2007;46:6113-17.
- [21] Shliomis MI. Ferrohydrodynamics: Retrospective and Issues. Berlin, Heidelberg; SpringerBerlin Heidelberg; 2002. p. 85-111. ISBN 978-3-540-45646-9.
- [22] Chen CY, Cheng ZY. An experimental study on Rosensweig instability of a ferrofluid droplet. Phys Fluids 2008;20(5):54105.
- [23] Lange A, Gollwitzer C, Maretzki R, Rehberg I, Richter R. Retarding the growth of the Rosensweig instability unveils a new scaling regime. Phys Rev E 2016;93:43106.
- [24] Lavrova O, Matthies G, Mitkova T, Polevikov V, Tobiska L. Numerical treatment of free surface problems in ferrohydrodynamics. J Phys Condens Matter 2006;18(38):S2657-69.
- [25] Lavrova O, Matthies G, Tobiska L. Numerical study of soliton-like surface configurations on a magnetic fluid layer in the Rosensweig instability. Commun Nonlinear Sci Numer Simul 2008;13(7):1302-10.
- [26] Yecko P. Stability of layered channel flow of magnetic fluids. Phys Fluids 2009;21(3):034102.
- [27] Yecko P. Effect of normal and parallel magnetic fields on the stability of interfacial flows of magnetic fluids in channels. Phys Fluids 2010;22(2):1-8.
- [28] Seric I, Afkhami S, Kondic L. Interfacial instability of thin ferrofluid films under a magnetic field. J Fluid Mech 2014;755:1-12.
- [29] Afkhami S, Renardy Y, Renardy M, Riffle JS, Pierre TGS. Field-induced motion of ferrofluid droplets through immiscible viscous media. J Fluid Mech 2008;610:363-80.
- [30] Afkhami S, Tyler AJ, Renardy Y, Renardy M, Pierre TGS, Woodward RC, et al. Deformation of a hydrophobic ferrofluid droplet suspended in a viscous medium under uniform magnetic fields. J Fluid Mech 2010;663:358-84.
- Rowghanian P, Meinhart CD, Campàs O. Dynamics of ferrofluid drop deformations under spatially uniform magnetic fields. J Fluid Mech 2016:802:245-62.
- [32] Wörner M. Numerical modeling of multiphase flows in microfluidics and micro process engineering; a review of methods and applications, Microfluid Nanofluid 2012:12(6):841-86.
- [33] Unverdi SO, Tryggvason G. A front-tracking method for viscous, incompressible, multi-fluid flows. | Comput Phys 1992;100(1):25-37.
- Tryggvason G, Bunner B, Esmaeeli A, Juric D, Al-Rawahi N, Tauber W, et al. A front-tracking method for the computations of multiphase flow. J Comput Phys 2001;169(2):708-59.
- 1351 Hirt CW, Nichols BD. Volume of fluid (VOF) method for the dynamics of free boundaries. J Comput Phys 1981;39(1):201-25.
- [36] Khismatullin D, Renardy Y, Renardy M. Development and implementation of VOF-PROST for 3D viscoelastic liquid-liquid simulations. J Non-Newton Fluid Mech 1992;140:120-31.
- Li J, Renardy YY, Renardy M. Numerical simulation of breakup of a viscous drop in simple shear flow through a volume-of-fluid method. Phys Fluids 2000;12(2):269-82.
- [38] Hua J, Lim LK, Wang CH. Numerical simulation of deformation/motion of a drop suspended in viscous liquids under influence of steady electric fields. Phys Fluids 2008;20(11):113302.
- [39] Korlie MS, A N, B G S, J G T, Trubatch AD, Yecko P. Modeling bubbles and droplets in magnetic fluids. J Phys Condens Matter 2008;20(20):204143.
- [40] Afkhami S, Cummings LJ, Griffiths IM. Interfacial deformation and jetting of a magnetic fluid. Comput Fluids 2016;124:149-56.
- [41] Sussman M, Smereka P, Osher S. A level set approach for computing solutions to incompressible two-phase flow. J Comput Phys 1994;114(1):146-59.
- [42] Sussman M, Fatemi E, Smereka P, Osher S. An improved level set method for incompressible two-phase flows. Comput Fluids 1998;27(5):663-80.
- [43] Sethian JA. Level set methods and fast marching methods. Cambridge Monographs on Applied and Computational Mathematics, 3. 2nd. Cambridge: Cambridge University Press; 1999.
- [44] Osher SJ, Fedkiw RP. Level set methods and dynamic implicit surfaces. Springer-Verlag; 2002.
- [45] Osher S, Fedkiw R. Level set methods and dynamic implicit surfaces, Applied Mathematical Sciences, 153. New York: Springer-Verlag; 2003.
- [46] Olsson E, Kreiss G. A conservative level set method for two phase flow. J Comput Phys 2005;210:225-46.
- [47] Olsson E, Kreiss G, Zahedi S. A conservative level set method for two phase flow II. J Comput Phys 2007;225:785-807.

- [48] Cahn JW, Hilliard JE. Free energy of a nonuniform system. I. Interfacial free energy. J Chem Phys 1958;28(2):258-67.
- [49] Cahn JW. Free energy of a nonuniform system. II. Thermodynamic basis. J Chem Phys 1959;30(5):1121-4.
- [50] Jacqmin D. Calculation of two-phase Navier-Stokes flows using phase-field modeling. J Comput Phys 1999;155(1):96-127.
- [51] Boyer F. Mathematical study of multi-phase flow under shear through order parameter formulation. Asymptot Anal 1999;20(2):175–212.
- [52] Liu C, Shen J. A phase field model for the mixture of two incompressible fluids and its approximation by a Fourier-spectral method. Physica D 2003;179(3-4):211-28.
- [53] Yue P, Feng J, Liu C, Shen J. A diffuse-interface method for simulating two-phase flows of complex fluids. J Fluid Mech 2004;515:293-317.
- [54] Kim J, Kang K, Lowengrub J. Conservative multigrid methods for Cahn-Hilliard fluids. J Comput Phys 2004;193(2):511-43.
- [55] Qian T, Wang X, Sheng P. A variational approach to the moving contact line hydrodynamics. [Fluid Mech 2006;564:333-60.
- [56] Gal CG, Grasselli M. Instability of two-phase flows: a lower bound on the dimension of the global attractor of the Cahn-Hilliard-Navier-Stokes system. Phys D 2011:240(7):629-35.
- [57] Cueto-Felgueroso L, Juanes R. A phase-field model of two-phase Hele-Shaw flow. J Fluid Mech 2014;758:522-52.
- [58] Gao Y, He X-M, Mei L, Yang X. Decoupled, linear, and energy stable finite element method for the Cahn-Hilliard-Navier-Stokes-Darcy phase field model. SIAM J Sci Comput 2018;40(1):B110-37.
- [59] Rebholz L, Wise S, Xiao M. Penalty-projection schemes for the Cahn-Hilliard Navier-Stokes diffuse interface model of two phase flow, and their connection to divergence-free coupled schemes. Int | Numer Anal Model 2018;15:649-76.
- [60] Yang X, Zhao J, He X-M. Linear, second order and unconditionally energy stable schemes for the viscous Cahn-Hilliard equation with hyperbolic relaxation using the invariant energy quadratization method. J Comput Appl Math 2018;343(1):80-97.
- [61] Ki H, Level set method for two-phase incompressible flows under magnetic fields, Comput Phys Commun 2010;181(6):999-1007.
- [62] Ghaffari A, Hashemabadi SH, Bazmi M. CFD simulation of equilibrium shape and coalescence of ferrofluid droplets subjected to uniform magnetic field, Colloids Surf A 2015:481:186-98.
- [63] Zhu GP, Nguyen NT, Ramanujan RV, Huang XY. Nonlinear deformation of a ferrofluid droplet in a uniform magnetic field. Langmuir 2011:27(24):14834-41.
- [64] Hadidi A, Jalali-Vahid D. Numerical simulation of dielectric bubbles coalescence under the effects of uniform magnetic field. Theor Comput Fluid Dyn 2016:30(3):165-84.
- [65] Wang X, Qian T, Sheng P. Moving contact line on chemically patterned surfaces. J Fluid Mech 2008;605:59-78.
- [66] He O, Glowinski R, Wang X, A least-squares/finite element method for the numerical solution of the Navier-Stokes-Cahn-Hilliard system modeling the motion of the contact line. J Comput Phys 2011;230(12):4991-5009.
- [67] Wang C, Wise SM. An energy stable and convergent finite-difference scheme for the modified phase field crystal equation. SIAM J Numer Anal 2011;49(3):945-69.
- [68] Feng X, Wise S. Analysis of a Darcy-Cahn-Hilliard diffuse interface model for the Hele-Shaw flow and its fully discrete finite element approximation. SIAM J Numer Anal 2012;50(3):1320-43.
- [69] Guo Z, Lin P, Lowengrub JS. A numerical method for the quasi-incompressible Cahn-Hilliard-Navier-Stokes equations for variable density flows with a discrete energy law. J Comput Phys 2014;276:486-507.
- [70] Nochetto RH, Salgado AJ, Walker SW. A diffuse interfce model for electrowetting with moving contat lines. Math Models Methods Appl Sci 2014;24(1):67-111.
- [71] Chen C, Yang X. Efficient numerical scheme for a dendritic solidification phase field model with melt convection. J Comput Phys 2019;388:41–62. [72] Chen C, Yang X. Fast, provably unconditionally energy stable, and second-order accurate algorithms for the anisotropic Cahn–Hilliard model. Comput Methods Appl Mech Eng 2019;351:35-59.
- [73] Feng X, Li Y, Xing Y. Analysis of mixed interior penalty discontinuous Galerkin methods for the Cahn-Hilliard equation and the Hele-Shaw flow. SIAM Numer Anal 2016;54(2):825-47.
- [74] Huang Q, Yang X, He X-M. Numerical approximations for a smectic-A liquid crystal flow model: first-order, linear, decoupled and energy stable schemes. Discrete Contin Dyn Syst Ser B 2018;23(6):2177-92.
- [75] Liu Z, Qiao Z. Wongzakai approximations of stochastic AllenCahn Eequation. Int | Numer Anal Model 2019;16:681-94.
- [76] Lin F, He X-M, Wen X. Fast, unconditionally energy stable large time stepping method for a new Allen-Cahn type square phase-field crystal model. Appl Math Lett 2019;92:248-55.
- [77] Chen M, Bollada PC, Jimack PK. Dynamic load balancing for the parallel, adaptive, multigrid solution of implicit phase-field simulations. Int J Numer Anal Model 2019:16:297-318.
- [78] Xu C, Chen C, Yang X, He X-M. Numerical approximations for the hydrodynamics coupled binary surfactant phase field model: second order, linear, unconditionally energy stable schemes. Commun Math Sci 2019;17(3):835-58.
- [79] Zhang J, Chen C, Yang X, Chu Y, Xia Z. Efficient, non-iterative, and second-order accurate numerical algorithms for the anisotropic Allen-Cahn equation with precise nonlocal mass conservation. I Comput Appl Math 2020;363:444-63.
- [80] Chen L, Zhao J, Yang X. Regularized linear schemes for the molecular beam epitaxy model with slope selection. Appl Numer Math 2018;128:139-56.
- [81] Yang J, Du Q, Zhang W. Uniform LP-Bound of the Allen-Cahn equation and its numerical discretization. Int J Numer Anal Model 2018;15:213–27.
- [82] Nochetto RH, Salgado AJ, Tomas I. The equations of ferrohydrodynamics: modeling and numerical methods. Math Mod Methods Appl Sci 2016:26(13):2393-449.
- [83] Gerbeau J-F, Le Bris C, Lelièvre T. Mathematical methods for the magnetohydrodynamics of liquid metals. Numerical Mathematics and Scientific Computation. Oxford: Oxford University Press; 2006. ISBN 978-0-19-856665-6; 0-19-856665-4.
- [84] Sermange M, Temam R. Some mathematical questions related to the MHD equations. Commun Pure Appl Math 1983;36(5):635-64.
- [85] Zhang G, He X-M, Yang X, Convergence analysis of an unconditionally energy stable projection scheme for magneto-hydrodynamic equations. Appl Numer Math 2019:136:235-56.
- [86] Zhang G, He X-M, Yang X. A decoupled, linear and unconditionally energy stable scheme with finite element discretizations for magneto-hydrodynamic equations. J Sci Comput 2019;81:16781711.
- [87] Zhang G, He X-M, Yang X. Decoupled, linear and unconditionally energy stable numerical scheme for a two-phase ferrohydrodynamics model. J Comput Appl Math 2020;369:112636.
- [88] Gunzburger MD, Ladyzhenskaya OA, Peterson JS. On the global unique solvability of initial-boundary value problems for the coupled modified Navier-Stokes and Maxwell equations. J Math Fluid Mech 2004;6(4):462-82.
- [89] Gunzburger MD, Meir AJ, Peterson JS. On the existence, uniqueness, and finite element approximation of solutions of the equations of stationary, incompressible magnetohydrodynamics. Math Comput 1991;56(194):523-63.
- [90] Cui W, Ou Y, Ren D. Incompressible limit of full compressible magnetohydrodynamic equations with well-prepared data in 3-D bounded domains. J Math Anal Appl 2015;427:263-88.
- [91] Hiptmair R, Li L, Mao S, Zheng W. A fully divergence-free finite element method for magnetohydrodynamic equations. Math Models Methods Appl Sci 2018;28(4):659–95
- [92] Ben Salah N, Soulaimani A, Habashi WG. A finite element method for magnetohydrodynamics. Comput Methods Appl Mech Eng 2001:190(43-44):5867-92
- [93] Ren X, Xiang Z, Zhang Z. Global well-posedness for the 2D MHD equations without magnetic diffusion in a strip domain. Nonlinearity 2016;29:1257-91.
- [94] Ren X, Xiang Z, Zhang Z. Global existence and decay of smooth solutions for the 3-D MHD-type equations without magnetic diffusion. Sci China Math 2016;59:1949-74.

- [95] Baňas L, Prohl A. Convergent finite element discretization of the multi-fluid nonstationary incompressible magnetohydrodynamics equations. Math Comput 2010;79(272):1957–99.
- [96] Prohl A. Convergent finite element discretizations of the nonstationary incompressible magnetohydrodynamics system. M2AN Math Model Numer Anal 2008;42(6):1065–87.
- [97] Ren X, Wu J, Xiang Z, Zhang Z. Global existence and decay of smooth solution for the 2-D MHD equations without magnetic diffusion. J Funct Anal 2014;267:503–41.
- [98] He Y, Zou J. A priori estimates and optimal finite element approximation of the MHD flow in smooth domains. ESAIM Math Model Numer Anal 2018;52(1):181–206.
- [99] Layton W, Tran H, Trenchea C. Numerical analysis of two partitioned methods or uncoupling evolutionary MHD flows. Numer Methods Partial Differ Equ 2014;30(4):1083–102.
- [100] Xiang Z. On the cauchy problem for the compressible Hall-magneto-hydrodynamics equations. J Evol Equ 2017;17:685-715.
- [101] Nochetto RH, Salgado AJ, Tomas I. A diffuse interface model for two-phase ferrofluid flows. Comput Methods Appl Mech Eng 2016;309:497–531.
- [102] Yang J, Mao S, He X-M, Yang X, He Y. A diffuse interface model and semi-implicit energy stable finite element method for two-phase magnetohydro-dynamic flows. Comput Methods Appl Mech Eng 2019;356:435–64.
- [103] Kim J. Phase-field models for multi-component fluid flows. Commun Comput Phys 2012;12(3):613-61.
- [104] Bai F, He X-M, Zhou R, Yang X, Wang C. Three dimensional phase-field investigation of droplet formation in microfluidic flow focusing devices with experimental validation. Int J Multiph Flow 2017;93:130–41.
- [105] Lim CY, Lam YC. Phase-field simulation of impingement and spreading of micro-sized droplet on heterogeneous surface. Microfluid Nanofluid 2014;17(1):131–48.
- [106] Shen J, Yang X. Decoupled, energy stable schemes for phase-field models of two-phase incompressible flows. SIAM J Numer Anal 2015;53(1):279-96.
- [107] Sussman M, Smereka P, Osher S. A level set approach for computing solutions to incompressible two-phase flow. J Comput Phys 1994;114(1):146-59.
- [108] Engquist B, Tornberg A-K, Tsai R. Discretization of dirac delta functions in level set methods. J Comput Phys 2005;207(1):28-51.
- [109] Tan S-H, Nguyen N-T, Yobas L, Kang TG. Formation and manipulation of ferrofluid droplets at a microfluidic t -junction. J Micromech Microeng 2010;20(4):45004.
- [110] Tan SH, Nguyen N-T. Generation and manipulation of monodispersed ferrofluid emulsions: the effect of a uniform magnetic field in flow-focusing and t-junction configurations. Phys Rev E 2011;84:36317.
- [111] Chen D, Huang T, Li L. Comparison of algebraic multigrid preconditioners for solving Helmholtz equations. J Appl Math 2012;2012:12. Article ID 367909.
- [112] Huang Z, Huang T. A constraint preconditioner for solving symmetric positive definite systems and application to the Helmholtz equations and Poisson equations. Math Model Anal 2010;15(3):299–311.
- [113] Le J. Jin H, Lv X, Cheng Q. A preconditioned method for the solution of the Robbins problem for the Helmholtz equation. ANZIAM J 2010;52:87–100.
- [114] Wu S, Huang T, Li L. Block triangular preconditioner for static Maxwell equations. Comput Appl Math 2011;30(3):589-612.
- [115] Wu S, Li C, Huang T. Modified block preconditioners for the discretized time-harmonic Maxwell equations in mixed form. J Comput Appl Math 2013;180(2):192-6.
- [116] Zhu L, Huang T, Li L. A hybrid-mesh hybridizable discontinuous Galerkin method for solving the time-harmonic Maxwell's equations. Appl Math Lett 2017;68:109–16.
- [117] De Menech M. Modeling of droplet breakup in a microfluidic T-shaped junction with a phase-field model. Phys Rev E 2006;73(3):31505.
- [118] Yang Q, Li BQ, Ding Y. 3D phase field modeling of electrohydrodynamic multiphase flows. Int J Multiph Flow 2013;57:1-9.
- [119] Minjeaud S. An adaptive pressure correction method without spurious velocities for diffuse-interface models of incompressible flows. J Comput Phys 2013;236:143–56.